LOW-COST AND FLEXIBLE USRP BASED REAL-TIME GLOBAL NAVIGATION SATELLITE SYSTEM RECEIVER FOR IONOSPHERIC SOUNDER

BY

DOYOUN KIM

THESIS

Submitted in partial fulfillment of the requirements
for the degree of Master of Science in Electrical and Computer Engineering
in the Graduate College of the
University of Illinois at Urbana-Champaign, 2017

Urbana, Illinois

Adviser:

Professor Jonathan J. Makela

ABSTRACT

Software defined radio (SDR) is a recent development in the wireless communication field that provides re-configurability and flexibility to the RF front end. We present a dual-frequency GNSS software receiver with an RF front end based on USRP N210 with DBSRX2. The USRP N210 with DBSRX2 can be used to receive L1C/A and L2CM signals. In this study, C++ class based GNSS-SDR software is selected to process navigation solutions for GPS L1 and L2C signals collected by the front end. When signals with two different frequencies penetrate a dispersive medium, such as the ionosphere, two different signal delays are created. Based on these delays, which can be calculated from the pseudorange and phase velocity result of the navigation solution, a total electron content (TEC) measurement is possible using the system that we develop.

To my parents, for their love and support.

ACKNOWLEDGMENTS

I would like to express my deep gratitude to Professor Jonathan J. Makela for his patient guidance, enthusiastic encouragement and useful critiques of this research work. I would also like to thank my research group members for their advice and assistance in keeping my progress on schedule. My grateful thanks are also extended to Mr. Smith for his help in supporting my research as a research mate. I would also like to extend my thanks to the technicians of the laboratory of the ECE department for their help in offering me the resources in running the program. Finally, I wish to thank my parents for their support and encouragement throughout my study.

TABLE OF CONTENTS

LIST OF TABLES

LIST OF FIGURES

LIST OF ABBREVIATIONS

ADC	Analog-to-Digital Converter
DAC	Digital-to-Analog Converter
DLL	Delay Lock Loop
FLL	Frequency Lock Loop
GNSS	Global Navigation Satellite System
GPSDO	GPS Disciplined Oscillator
GPS	Global Positioning System
L1C/A	L1 Coarse/Acquisition
L2C	L2 Civilian
NF	Noise Figure
OXCO	Oven Controlled Crystal Oscillator
PLL	Phase Lock Loop
PPM	Parts Per Million
PRN	Pseudorandom Number
RF	Radio Frequency
RX	Receiver
SA	Select Availability
SDR	Software Defined Radio
TCXO	Temperature Controlled Crystal Oscillator
TOW	Time of Week
USRP	Universal Software Radio Peripheral

CHAPTER 1

INTRODUCTION

Up to the present day, industry has made many advances in the communication and navigation field, but the solutions that have been created typically work on integrated chips which do not have the capability to adjust their performance and use fixed parameters such as center frequency and sampling frequency. In 1993, software defined radio (SDR) technology was introduced, and due to its flexibility, re-configurability, and reasonable cost, an SDR draws attention to various fields that require real-time adjustments of parameters such as signal amplitude and sampling frequency (Mitola, 1993)[1]. The next generation of wireless communication, 5G, and the Global Navigation Satellite System (GNSS) are two examples of the potential use of SDR as part of the radio frequency (RF) front end. One of the key requirements for 5G is enhanced radio functionality such as array antenna beam forming. Due to its high frequency and high loss in the propagation channel, antenna beam forming at the RF front-end is challenging and it requires a flexible adaptation to the environment by changing its parameters. The attention on 5G research based on the SDR is well presented in Felita and Suryanegara, 2013 [2], Xiong et al., 2014 [3], Kaltenberger et al., 2015 [4], and Mathur et al., 2017 [5]. Researchers use the GNSS signals not only for navigation solutions but also for various purposes such as monitoring the ionopshere. As demand increases, the flexibility of receivers draws attention to the possibilities of dynamically modifying the tracking loop to allow navigation under demanding conditions and of utilizing new and modern signals. The development of a GNSS receiver based on the SDR was introduced by Akos, 1997 [6] and Borre et al., 2005 [7]. Several more approaches, such as multi-constellation and multi-frequency receivers, were developed by Peng and Morton, 2013 [8] and Presti et al., 2014 [9].

Since the ionosphere is a dispersive medium, propagation through it will affect the electromagnetic signals broadcast by the GNSS satellites. Given

the impact of the ionosphere on the GNSS signals, these signals provide an excellent tool for ionospheric monitoring. Therefore, several approaches have performed total electron content measurements based on GNSS signals (Fernandez-Prades et al., 2001 [10], Dyrud et al., 2008 [11], Shanmugam et al., 2012 [12], and Romano et al., 2013 [13]). GPS receivers have been employed by researchers for investigation into ionospheric and atmospheric science for the past three decades, yet a number of improvements in measurement accuracy and flexibility are necessary for today's applications (Ganguly et al., 2002 [14] and Linty et al., 2015 [15]).

In this work, we develop a low-cost and flexible ionospheric sounder using SDR. Two almost identical system setups using SDR have been built to track signals at two different GPS frequencies: GPS L1 at 1575.62 MHz, and GPS L2 at 1227.6 MHz. By simultaneously tracking these two signals, the dual-SDR system would have the capability to monitor the ionosphere electron density (Jovancevic et al., 2001) [16]. The SDR is implemented on a universal software radio peripheral (USRP) system, which allows rapid adaptation to the measurement needs.

In Chapter 2, the GNSS receiver setup starts with the implementation of a USRP-based GNSS receiver for the GPS L1 and L2 signals, which use USRP N210 with the DBSRX daughterboard. An active antenna, splitter, low noise amplifier, and external clock are required for GPS signal reception, and this signal is fed into the daughterboard and the USRP. The open source software GNSS-SDR is selected to draw out a navigation solution from the digitized data fed from the USRP. Using the system with two USRPs, one for the L1 and one for the L2 signal, the results of the navigation solution have been demonstrated and are shown in Chapter 3. The signal plan for the L1 and L2 signals, and measurement results, are given to explain the result of the navigation solutions. The importance of each measurement will be discussed. In Chapter 4, total electron content is derived from the GPS measurements. Actual TEC measurement from dual-SDR system and challenges will be discussed. Finally, a summary of current and future work is presented in Chapter 5.

CHAPTER 2

IMPLEMENTATION OF A USRP BASED REAL-TIME GLOBAL NAVIGATION SATELLITE SYSTEM (GNSS) RECEIVER

The USRP based real-time GNSS receiver comprises three main components: (1) RF front-ends, (2) universal software radio peripheral (USRP), and (3) navigation solution algorithm. A basic signal flow graph of the overall system from GPS satellite to navigation solution is shown in Figure 2.1. Two USRPs are used because this system is designed to operate as an ionospheric sounder, requiring operation at two different frequencies, L1 at 1575.62 MHz, and L2 at 1227.6 MHz. More details on the ionospheric sounding capabilities are given in Chapter 4. Therefore, all of the receiver setup and key features are focused on receiving these two signals.

The main purpose of the RF front-ends is to properly receive the GNSS signal from the GNSS satellite and deliver a filtered and properly amplified signal to the USRP. In the USRP, the analog signal is digitized, sampled, and then fed to the navigation solution algorithm. In this thesis, a GNSS-SDR software navigation algorithm is employed [10]. These three components are discussed in terms of developing a flexible GNSS receiver in this chapter. Actual measurements will be discussed in Chapter 3.

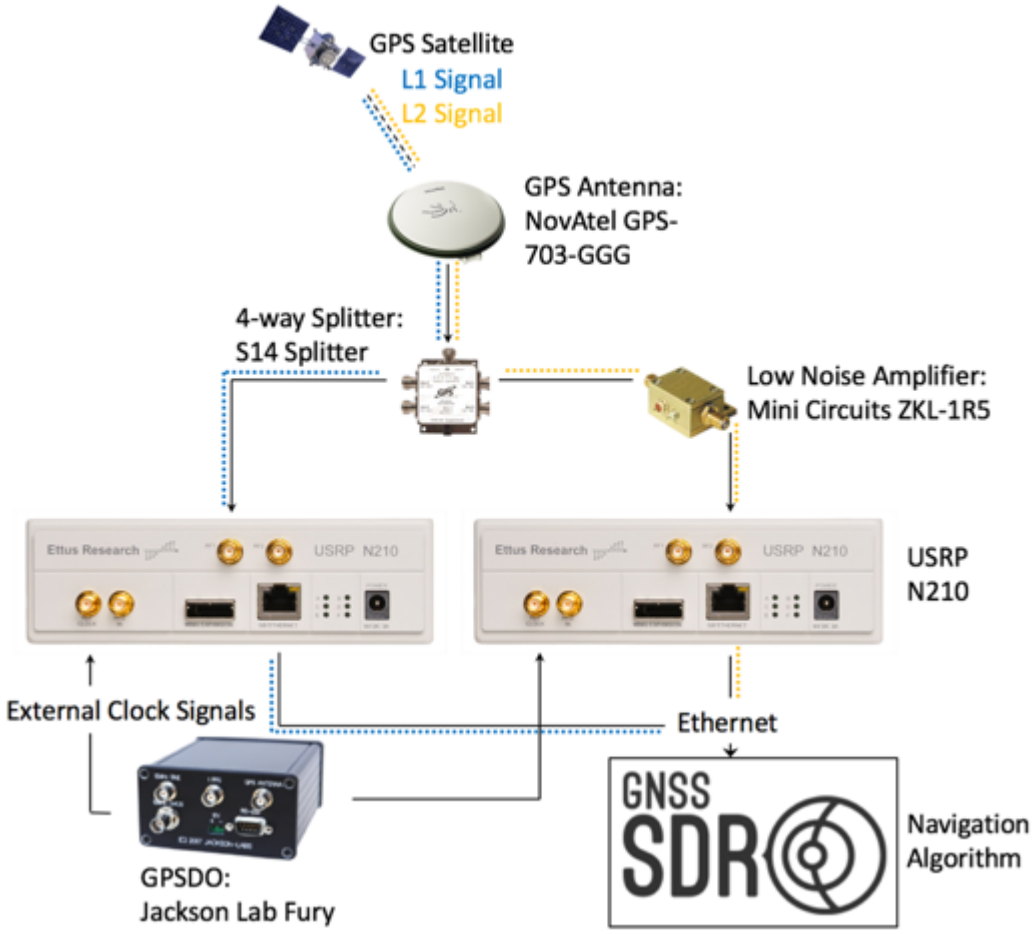

Figure 2.1: Overall System Implementation

2.1 RF Front-Ends

The RF front-ends are generally defined as everything between the receive antenna and the digital baseband system, where a continuous RF signal is converted to discrete digitized data at the zero center frequency. The GNSS receiver consists of five components: (1) active GPS antenna, (2) 4-way splitter, (3) low noise amplifier, (4) daughterboards and (5) external clock. Key features and performance of each component will be explained as well as its significance in order to develop the flexible GNSS system.

Figure 2.2: Actual RF Setup

2.1.1 Active GPS Antenna

Figure 2.1 and Figure 2.2 show the configuration of the GNSS receiver which was actually set up in the RF Lab in the Department of Electrical and Computer Engineering at the University of Illinois at Urbana-Champaign. The GNSS signal is captured by the NovAtel GPS-703-GGG antenna which is an active antenna. Two of these antennas are installed on the roof of the Electrical and Computer Engineering Building: one antenna on the East (called GPS Blue) and the other on the West (called GPS Red). Three important features for the active antenna are frequency range, antenna gain and noise figure. The NovAtel antenna is capable of receiving the GPS L1 (1580.0+/−28.5 MHz), L2 (1210.0+/−45.0 MHz), and L5 (1210.0+/−45.0 MHz) frequencies. The gains for the antenna are 5 dBic, 3 dBic and 3 dBic for L1, L2, and L5, respectively, with a typical noise figure of 2 dB. Antenna gain patterns at each frequency are shown in Figure 2.3. Noise figure is the special feature for active devices that amplifies the signal, and it represents how much noise will be added while the signal is amplified. In the process of building an RF system, noise figure is a significant feature that determines noise power of the system. If the GNSS signal power is below the noise power, the system will be unstable. Based on the Friis equation in Equation 2.2, total noise figure is dominated by the first active device of the signal. Since the active antenna is the first active device in our system to amplify the signal, it plays a significant role for the total cascade noise figure of the

system, as seen in Equations 2.1 and 2.2:

$$NF = 10log_{10}F = \frac{SNR_{in}}{SNR_{out}} \tag{2.1}$$

$$F_{total} = F_1 + \frac{F_2 - 1}{G_1} + \frac{F_3 - 1}{G_1 G_2} \ldots \tag{2.2}$$

where:

- NF is the noise figure
- F is the noise factor
- G is the gain of the component
- F_{total} is total noise factor

F_{total} is dominated by the first component of noise factor F_1 and gain G_1, which is from the active antenna of this system, $10^{2/10}$ (from typical noise figure 2 dB) and 5 dBic in the L1 case.

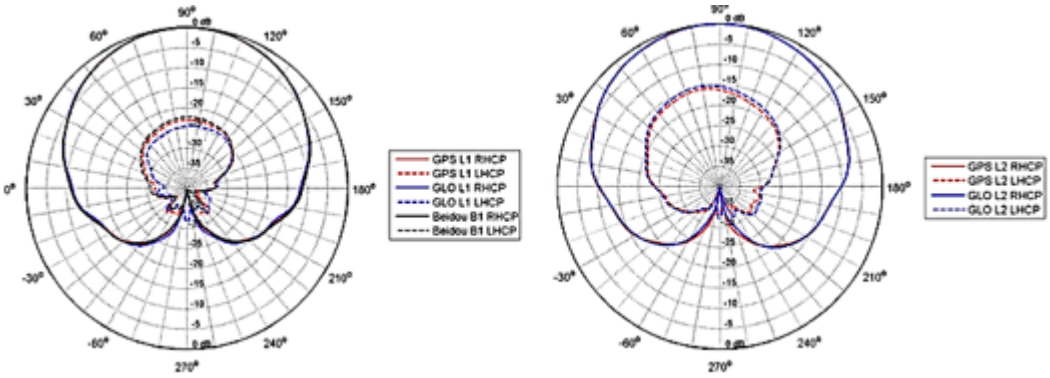

Figure 2.3: NovAtel GPS-703-GGG Antenna Gain Pattern (reprinted from [17])

2.1.2 4-way Splitter

The active antenna is connected to about 150 feet of coaxial cable and fed into a 4-way splitter manufactured by GPS Source. It has a wide frequency range from 1 GHz to 2 GHz with a flattened frequency response with about

7 dB loss, as shown in Figure 2.4. It splits the signal into four in order to provide each bench in the lab with the GPS signal. In this thesis, two outputs from the 4-way splitter are used, as shown in Figure 2.1, to feed the signal into the specific USRP used to separately process the L1 and L2 signals.

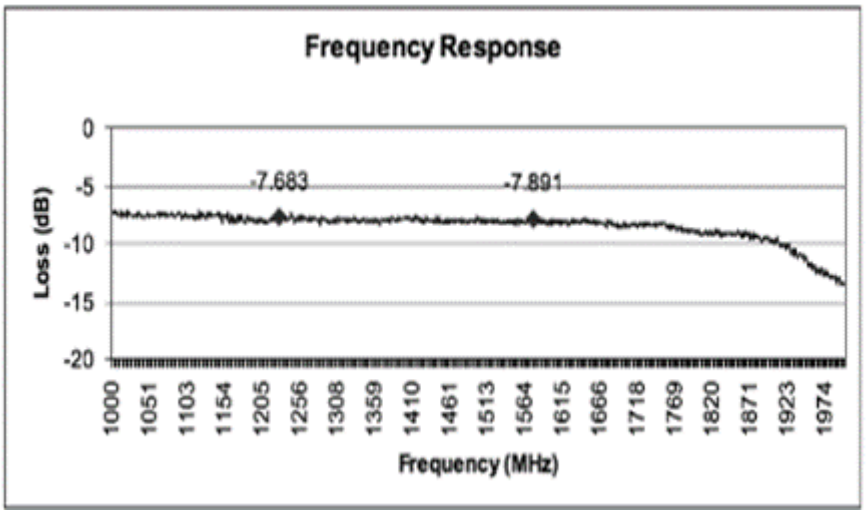

Figure 2.4: 4-way Splitter Performance (reprinted from [18])

2.1.3 Low Noise Amplifier

The L2 signal is about 30 dB lower at the end of the 4-way splitter output of the USRP measurement. Therefore, an additional low noise amplifier is required in order to have sufficient carrier-to-noise ratio (C/N0) while suppressing noise. Three main features for the amplifier are frequency, gain, and noise figure. The L2 signals that come out of one of the splitters are fed into a wideband Mini-Circuits ZKL-1R5 amplifier (frequency range: 10-1500 MHz) with maximum gain of 40 dB and low noise figure of 3 dB, as shown in Figure 2.5. C/N_0 is calculated as:

$$C/N_0 = C(N - BW) = C - N_0 = SNR + BW \tag{2.3}$$

where:

- C is the carrier power in dBm
- N is the noise power in dBm

- N_0 is the noise power density in dBm-Hz
- BW is the bandwidth of observation

Typically, C/N_0 for L1 C/A code is about 37 to 45 dB-Hz and L2 is about 30 dB lower than the L1 signal. The significance of the C/N_0 in a GPS receiver is in evaluating the performance of the RF front-end bandwidth, acquisition, and tracking stage. Actual measurements will be reported in Chapter 3.

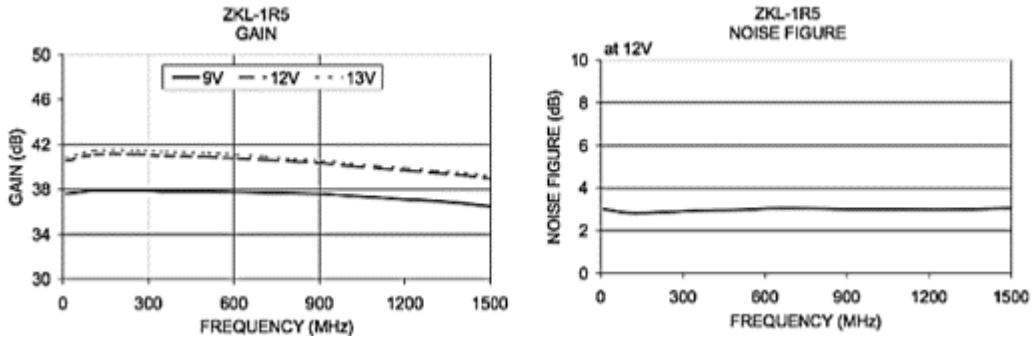

Figure 2.5: Amplifier Performance (reprinted from [19])

2.1.4 GPSDO External Clock

A GPS disciplined oscillator (GPSDO) was required for this work not only due to the high precision stability reference requirements but also due to the need for synchronization of the two USRPs in order to work with the L1 and L2 signals. For this purpose, we used an external GPSDO instead of using the USRP N210 internal TCXO (temperature controlled crystal oscillator) which has a frequency accuracy limitation up to 2.5 ppm. The L2 signal has a longer code period, which requires higher frequency precision than that provided by the USRP. Therefore, the Jackson Lab Fury is selected as the GPSDO, which creates its reference with an OXCO (oven controlled crystal oscillator). The OCXO is 100 times more accurate than the TCXO, at about 0.025 ppm as shown in Figure 2.6, where the Allen Deviation represents stability of a frequency over certain time period. The OCXO outputs a 10 MHz signal which will discipline the TCXO on the motherboard.

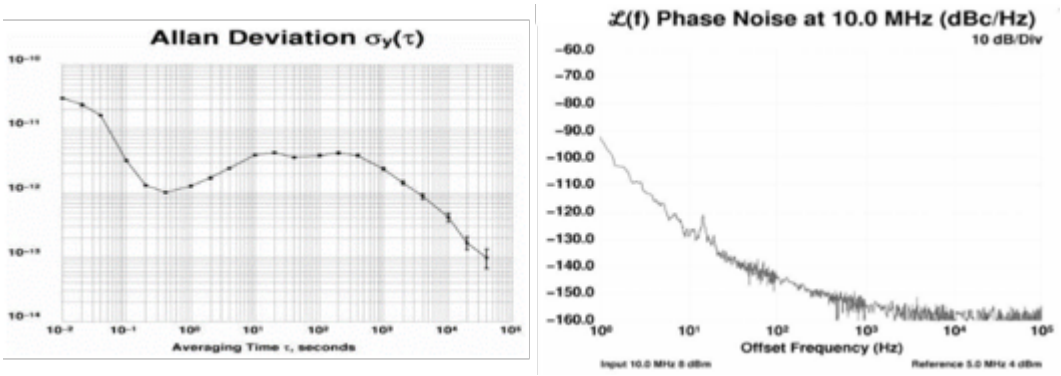

Figure 2.6: GPSDO Performance (reprinted from [20])

2.1.5 Daughterboards

The daughterboard performs signal mixing using a local oscillator. We categorized it as a part of the RF front-end since the signal is still analog at the output of this component. Second generation USRP models, such as the N210 selected in this work , require external transceiver daughterboards. There are a variety of daughterboards allowing GNSS signal reception as shown in Table 2.1. In this thesis, DBSRX2 is selected due to its reasonable frequency coverage (800 MHz - 2.3 GHz) and high range RX gain. Since the signal of the input to this stage is already amplified from the previous stages, the gain magnitude provided by the daughterboard does not contribute actual signal amplification. However, P1dB compression point of the amplifier needs to be figured out where its non-linearity region starts as that creates signal degradation. For example, if the received signal power exceeds the P1dB of the daughterboard amplifier, then the signal will be degraded due to the amplifier's limit.

2.2 USRP Software Defined Radio

The term software defined radio (SDR) was coined by Joseph Mitola from MITRE Corporation in 1991[1]. The term refers to a radio system in which all signal modulation and processing is done in software instead of hardware. The USRP is a flexible low-cost platform for SDRs developed by Matt Ettus. Some USRP models such as B200, B210 or E310 have an embedded/integrated transceiver. Specifications for each model are listed in Tables

Table 2.1: Possible Daughterboards for GNSS Application

Daughterboards	**Freq. Coverage**	**Analog BW**	**RX Gain**
WBX-120	50 MHz - 2.2 GHz	120 MHz	0 - 31.5 dB
SBX-120	400 MHz - 4.4 GHz	120 MHz	0 - 31.5 dB
CBX-120	1.2 GHz - 6.0 GHz	120 MHz	0 - 31.5 dB
UBX-160	10 MHz - 2.2 GHz	160 MHz	0 - 31.5 dB
WBX	50 MHz - 2.2 GHz	40 MHz	0 - 31.5 dB
SBX	400 MHz - 4.4 GHz	40 MHz	0 - 31.5 dB
CBX	1.2 GHz - 6.0 GHz	40 MHz	0 - 31.5 dB
UBX-40	10 MHz - 6.0 GHz	40 MHz	0 - 31.5 dB
DBSRX2	800 MHz - 2.3 GHz	8 - 80 MHz	0 - 73 dB,0 - 15 dB

2.2 and 2.3. There are a variety of USRP models with different specifications, and mixing and matching different daughterboards (in Table 2.1) will cover a wide range of performances shown in Table 2.4.

Table 2.2: Possible USRP Models for GNSS Application

USRP Model	**RF BW**	**RX Gain**	**ADC BW**
USRP1, B100	0 - 8 MHz	Daughterboard Gain	64 MS/s
B2xx	200 kHz - 56 MHz	0 - 73 dB	61.44 MS/s
N2xx	0 - 25 MHz	Daughterboard Gain	100 MS/s
X300, X310	0 - 120 MHz	Daughterboard Gain	200 MS/s

Table 2.3: Possible USRP Models for GNSS Application

USRP Model	**Interface**	**Host Sample Rate**
USRP1, B100	USB 2.0	8 MS/s
B2xx	USB 3.0	61.44 MS/s
N2xx	10 Gb Ethernet	25 MS/s
X300, X310	10 Gb Ethernet	200 MS/s

In this thesis, we select the USRP N210, which consists of two main boards: one for the receiver and one for the transmitter. The motherboard consists of a 14-bit high precision analog-to-digital converter (ADC) and digital-to-analog converter (DAC) to allow for capturing a wide-band signal covering a wide dynamic range.

The USRP is based on the design of the FPGA, which is a reprogrammable piece of hardware, and this enables high-speed signal processing. The FPGA used in the USRP is the Spartan 3A-DSP 3400 FPGA. The FPGA config-

uration implements down-conversion of the incoming signal to a zero center frequency, decimates the sampled signals, filters out-of-band components, and finally transmits them through a packet router to the Ethernet port. The DBSRX2 is mounted on the receiver motherboard as in Figure 2.7 and its performance is compared with different mixtures of daughterboard and USRP for GNSS signal in Table 2.4. In section 2.3, signal parameters (i.e., center frequency and sampling frequency) will be determined/controlled by the part of algorithm from the software side.

Table 2.4: USRP with Daughterboards for GNSS Application

Spec	**N210+DBSRX2**	**X310+WBX**	**B210+WBX**
Bandwidth	25 MHz	120 MHz	56 MHz
Center Freq.	0.8 - 2.35 GHz	0.05 - 2.2 GHz	0.05 - 2.2 GHz
Constellation	GPS/GLONASS	GPS/GLONASS	GPS/GLONASS
Sampling Freq.	0 - 25 MS/s	Up to 25 MS/s	Up to 25 MS/s
Quantization	14 bit	14 bit	14 bit
DC Power	6 V	6 V	6 V
RX Gain	15 dB	31.5 dB	104.5 dB
Supported OS	Linux/Mac/Win	Linux/Mac/Win	Linux/Mac/Win
Cost	$ 2064.00	$ 5926.00	$ 1852.00

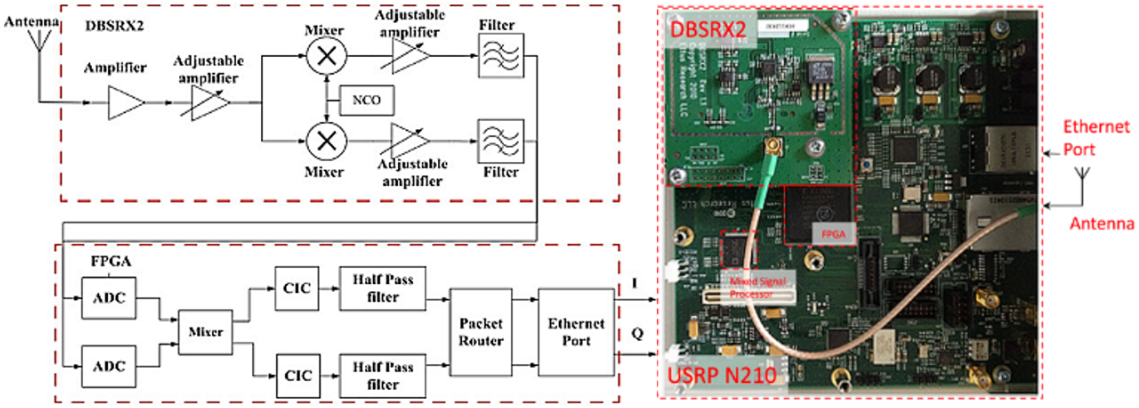

Figure 2.7: USRP N210 and DBSRX2 Internal Structure

2.3 Navigation Solution Algorithm

The parameters that control the USRP and overall navigation solution algorithm are defined in the software. This software is called GNSS-SDR [10] and it comprises two main portions shown in Figure 2.8: (1) Control Plane, creating a flowgraph, and (2) Signal Processing Plane, which consists of signal processing blocks.

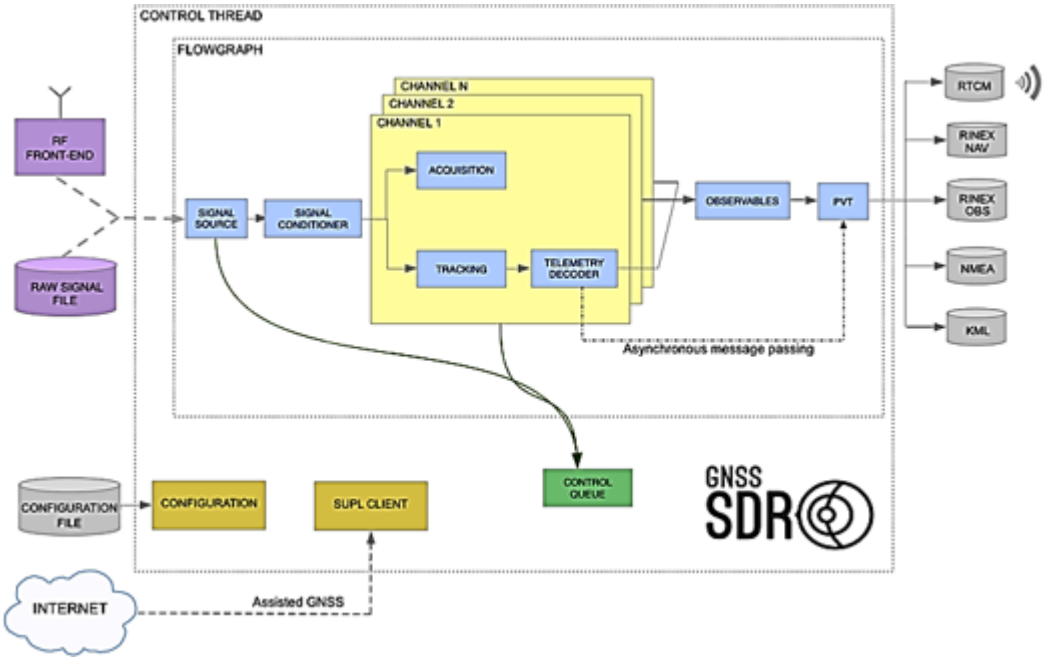

Figure 2.8: GNSS SDR Overall Flowgraph (reprinted from [10])

2.3.1 Control Plane

The Control Plane is in charge of creating a flowgraph based on the user-specified configuration. The configuration allows the users to customize their receivers by specifying the flowgraph using a .conf file (i.e., signal source, number of channels, satellite selections). This feature gives users a lot of flexibility in setting up the USRP to suit needs. There are two implementations of this interface: FileConfiguration and InMemoryConfiguration. FileConfiguration reads in pairs of property names and values from the configuration .conf file and stores them internally. For example, if we want to set the USRP Sampling.frequency from SignalSource module to 2 MHz, the following line

should be in the configuration .conf file.

```
SignalSource.sampling_frequency=2000000
```

InMemoryConfiguration, which is not from the .conf file, is for test purposes to avoid file dependency. The ControlThread class in Figure 2.8 is in charge of initiation for the GNSSFlowgraph and passing the required configuration. Once the flowgraph is launched and its signal processing blocks connected by Control Plane, it starts to process the incoming data stream from the USRP Ethernet port.

2.3.2 Signal Processing Plane

Class hierarchy of the C++ object-oriented programing language used in GNSS-SDR is an essential aspect which is described in Figure 2.9. The classes are described as rectangles with two sections: the top section for the name of the class, and the bottom section for the methods of the class. A dashed arrow from one class to the other represents the dependency relationship. Figure 2.9 explains the definition of different algorithms and different implementations that are initiated based on the configuration. Details about the configuration will be explained in the following sections using examples of receiving L1 C/A code.

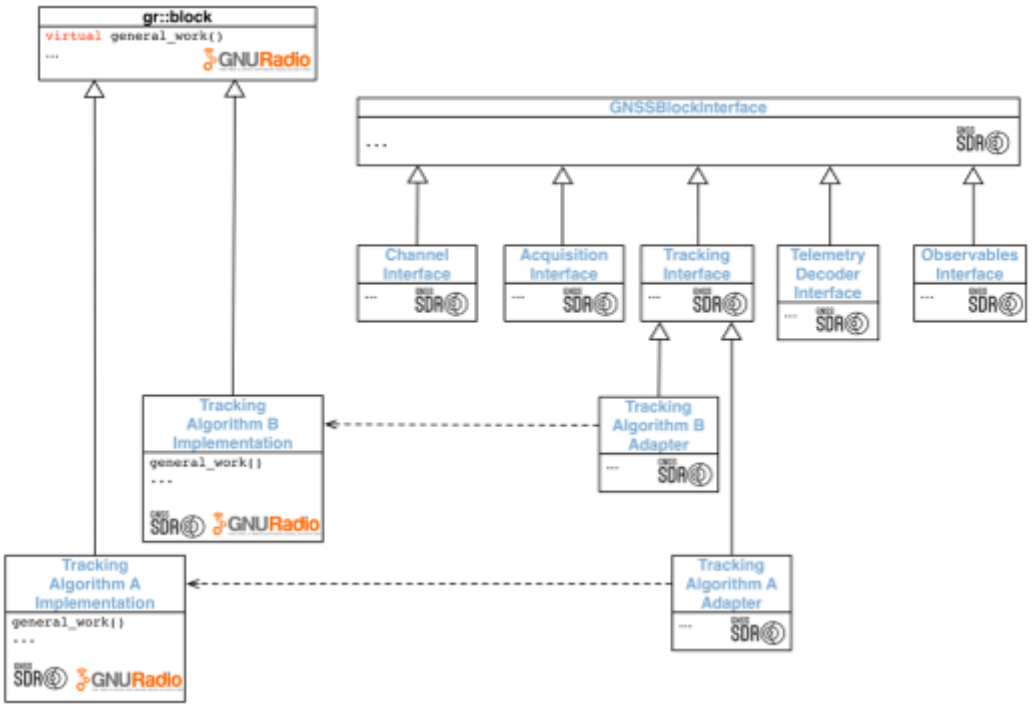

Figure 2.9: Signal Processing Class Hierarchy (reprinted from [10])

2.3.3 Signal Source

The Signal Source module is in charge of implementing the USRP hardware driver in order to operate the RF front-end with proper parameters and receiving the data coming from the ADC. This operation takes place through the Ethernet port of the USRP. Relevant parameters of the received signal, such as the center frequency, sampling frequency, and device setup, must be defined by the user in the signal source section of the configuration file. The following configuration is the basic setup for receiving L1 signal in real-time.

```
;########## SIGNAL_SOURCE CONFIG ##############
SignalSource.implementation=UHD_Signal_Source
SignalSource.device_address=192.168.40.2
SignalSource.item_type=gr_complex
SignalSource.sampling_frequency=2000000
SignalSource.freq=1575420000
SignalSource.gain=60
SignalSource.subdevice=A:0
```

```
SignalSource.samples=0
SignalSource.repeat=false
SignalSource.dump=false
SignalSource.dump_filename=../data/signal_source.dat
SignalSource.enable_throttle_control=false
```

2.3.4 Signal Conditioner

The Signal Conditioner is in charge of the Data Type Adapter, Input Filter, and Resampler. The Data Type Adapter, which is the first processing block in the Signal Conditioner block as shown in Figure 2.10, performs a conversion of the data type on the incoming data stream. It provides several implementations of data type conversion based on user preference (i.e., bytes, short, float). The second processing block, Input Filter, is a digital filter. There are two kinds of filter implementation available: finite impulse response filter and adaptive filter. The last processing block is Resampler, which resamples the signal to deliver it to the parallel processing channel blocks.

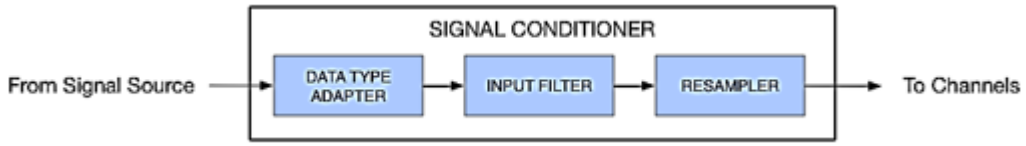

Figure 2.10: Signal Conditioner

2.3.5 Channel

Each channel comprises the acquisition, tracking, and decoding blocks. The number of channels is defined in the .conf file. The following configuration is an example of the channel configuration for the L1 signal. There are six channels, which create six parallel blocks; more channels mean a bigger computational burden. Channels.in_acquisition defines the number of acquisition blocks. Due to different Doppler frequencies, each satellite has a different signal plan for its data structure. Channel.signal=1C represents the L1 signal

and 2S represents the L2 signal.

```
Channels_1C.count=6
Channels.in_acquisition=1
Channel.signal=1C
```

2.3.6 Acquisition

The very first task of the receiver is to figure out the presence or absence of the satellites in view in a process called acquisition. The Acquisition block provides two estimated signal parameters to the tracking loop: coarse frequency of Doppler shift and code delay of the local code for alignment with the incoming signal. The parameters in the following configuration are an example Acquisition block setup. The core of the acquisition block is the implementation, GPS_L1_CA_PCP_Acquisition, which consists of the correlation algorithm.

```
;########## ACQUISITION GLOBAL CONFIG ############
Acquisition_1C.dump=false
Acquisition_1C.dump_filename=./acq_dump.dat
Acquisition_1C.item_type=gr_complex
Acquisition_1C.if=0
Acquisition_1C.coherent_integration_time_ms=1
Acquisition_1C.implementation=GPS_L1_CA_PCPS_Acquisition
Acquisition_1C.threshold=0.01
Acquisition_1C.doppler_max=10000
Acquisition_1C.doppler_step=500
Acquisition_1C.bit_transition_flag=false
Acquisition_1C.max_dwells=1
```

2.3.7 Tracking

If the Acquisition block finds a specific GPS signal, the estimated parameters are fed to the receiver tracking block. This block performs a local search

for accurate estimates of code delay and carrier frequency by employing a delay lock loop (DLL) for code delay tracking, in addition to a phase lock loop (PLL) and frequency lock loop (FLL) for carrier tracking. As shown in the following example, the core configuration parameter is implemented in GPS_L1_CA_DLL_PLL_Tracking, which contains the tracking algorithm while other parameters are adjustable for better reception. Also, this block allows the collection of tracking results into a file by enabling dump parameter, which is very helpful to determine receiver performance. The file contains in-phase and quadrature, PRN, carrier frequency, and C/N_0 results.

```
;########## TRACKING GLOBAL CONFIG ##############
Tracking_1C.implementation=GPS_L1_CA_DLL_PLL_Tracking
Tracking_1C.item_type=gr_complex
Tracking_1C.if=0
Tracking_1C.dump=false
Tracking_1C.dump_filename=./tracking_ch_
Tracking_1C.pll_bw_hz=30.0;
Tracking_1C.dll_bw_hz=4.0;
Tracking_1C.order=3;
Tracking_1C.early_late_space_chips=0.5;
```

2.3.8 Decoding of Navigation Message

This block is where the transmitted messages are decoded to yield the ephemeris and almanac orbital parameters of satellites. As shown in the following example, configuration parameter is very concise since this block is dealing with digital data from the Tracking block. Navigation data bits are structured into words, pages, subframes, frames, and superframes.

```
;########## TELEMETRY DECODER GPS CONFIG ##############
TelemetryDecoder_1C.implementation
                    =GPS_L1_CA_Telemetry_Decoder
TelemetryDecoder_1C.dump=false
TelemetryDecoder_1C.decimation_factor=1;
```

2.3.9 Observable

The most commonly used GPS observable is the pseudorange. Due to several error terms, the actual range measurement made by a receiver is the true pure range observation with the addition of various error terms. The pseudorange is computed from the outputs of the tracking block and the decoding of the navigation message. This block collects all the data provided by every channel that is tracked, aligns all received data into a coherent set and computes the pseudoranges. Also, this block allows the collection of the result from the observable block into a file by enabling the dump parameter shown in the following example. The file contains TOW, PRN, and pseudorange information. Using this pseudorange observation at two frequencies, the dual frequency ionospheric sounder can be built as shown in Chapter 4.

```
;########## OBSERVABLES CONFIG ############
Observables.implementation=Hybrid_Observables
Observables.dump=false
Observables.dump_filename=./observables.dat
```

CHAPTER 3

RESULTS OF NAVIGATION SOLUTION DETERMINATION

Under the modernized GPS, there are four signals available for civilian use: L1 C/A, L2C, L5, and L1C. Three of these represent new navigation signals designed for civilian use: L2C, L5, and L1C. In this work, we focus on the GPS L1 C/A signal and GPS L2C signal since these have the highest availability in number of satellites transmitting signals. Therefore, this chapter begins with the properties of the GPS L1 and L2 signals. Based on the setup of the previous chapter, the configurations for the L1 C/A signal and L2C signal will be defined for the receiver in section 3.1 and the results of acquisition and tracking will be explained in section 3.2. Lastly, a discussion of the result from the Tracking and Observable block is given in section 3.3. The major focus of the Observable block will be generating the pseudorange measurement from which a navigation solution can be calculated. The general technique to measure pseudorange and the results of the measurement will be discussed.

3.1 L1 and L2 Signal Plan

3.1.1 L1 Signal Plan

The GPS L1 signal is the most widely used signal for navigation purposes. Three signals are currently transmitted on GPS L1, centered at carrier frequency of 1575.42 MHz: C/A code, P(Y) code, and M-Code in Figure 3.1. The legacy civil signal, called L1 C/A (coarse acquisition) or C/A at L1, is the best known as most civilian receivers in use today are based on it. The L1 C/A has been continuously broadcast since 1993. The L1 C/A signal was open from the very beginning of the GPS program. It is transmitted by the IIR, IIR-M and IIF block satellites with PRN chipping frequency of 1.023

MHz and total chip length of 1023. The technical characteristics of the L1 C/A signal are summarized in the second column of Table 3.1 [21]. Based on these technical characteristics, the RF front-end setup and configurations for the navigation algorithm are defined as in section 3.1.2 for L1C/A and in section 3.1.4 for L2CM.

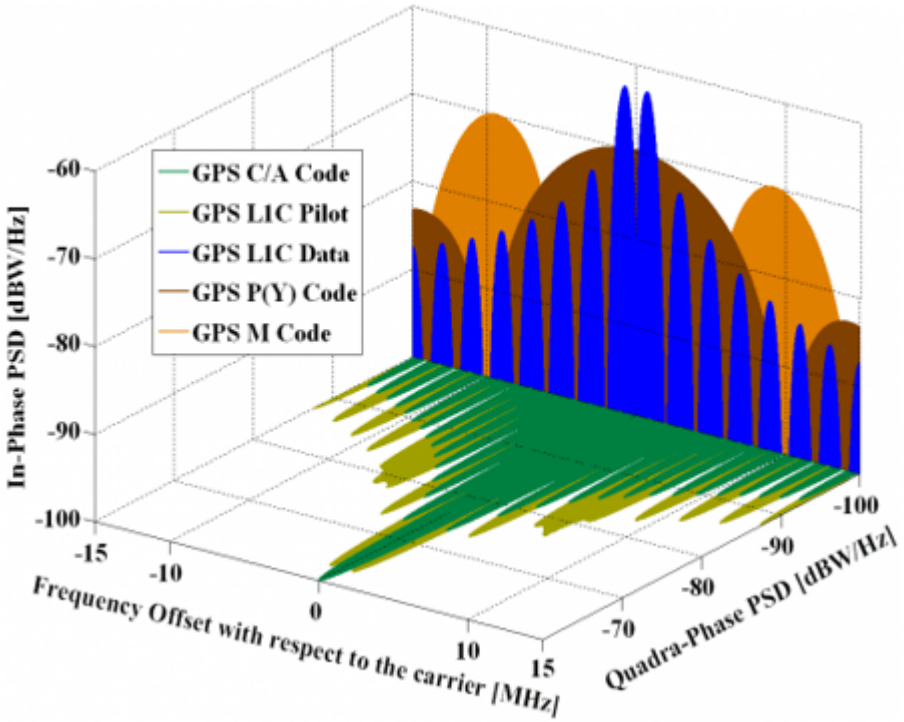

Figure 3.1: L1 Signal Spectrum

Table 3.1: L1 and L2 Signal Plan

Signal	**L1**	**L2**
GNSS System	GPS	GPS
Service Name	L1 C/A	L2 CM
Center Frequency	1575.42 MHz	1227.60 MHz
Frequency Band	L1	L2
Access Technique	CDMA	CDMA
Signal Component	Data	Data
Modulation	BPSK(1)	BPSK(1)
Code Frequency	1.025 MHz	511.5kHz
PRN Code Length	1023 (1 ms)	10230 (20 ms)
Code Family	Gold Code	M-sequence
Data Rate	50 bps/ 50 sps	25 - 50 bps/ 50 sps
Min. Received Power	-158.5 dBW	-164.5 / -161.5 dBW
Evaluation	5 degree	5 degree

3.1.2 L1 Signal Configurations

The following source code specifies the configurations for receiving the L1 C/A signal, and general information about each block is given in section 2.3. Comments are attached inside of the source code for important details.

```
[GNSS-SDR]

;########## GLOBAL OPTIONS ##################
GNSS-SDR.internal_fs_sps=2000000
;Comment: internal_fs_sps - Internal signal sampling freq
                after the signal conditioning stage [Hz].

;########## SIGNAL_SOURCE CONFIG #############
SignalSource.implementation=UHD_Signal_Source
; Comment: implementation - [UHD_Signal_Source] is chosen
        since we use the USRP to collect data
        and analyze data in real time.

SignalSource.device_address=192.168.40.2
;Comment: USRP address needs to be specified.

SignalSource.item_type=gr_complex
```

```
;Comment: item_type- Type and resolution
        for each of the signal samples.

SignalSource.sampling_frequency=2000000
;Comment: sampling_frequency is chosen 2 MHz
        because of L1 C/A bandwidth.

SignalSource.freq=1575420000
;Comment:freq is chosen 1.57542 GHz
                which is L1 center frequency.
SignalSource.gain=60
;Comment: gain is set to 60 dB at the daughterboard.
SignalSource.subdevice=A:0
;Comment: subdevice is RX portion of the USRP.

SignalSource.clock_source=external
;Comment: since we synchronize two USRPs with GPSDO,
        clock_source needs to be external

SignalSource.samples=0
;Comment: samples- Number of samples to be processed.
        Notice that 0 indicates the entire file.

SignalSource.repeat=false
;Comment: repeat- Repeat the processing file.

SignalSource.dump=false
SignalSource.dump_filename=../data/signal_source.dat
;Comment: dump- Dump the Signal source data to a file.
        Disable this option in this version.

SignalSource.enable_throttle_control=false
;Comment: enable_throttle_control- Enabling this option
        tells the signal source to keep the delay
        between samples in post processing.
        It helps to not overload the CPU,
```

```
        but the processing time will be longer.

;########## SIGNAL_CONDITIONER CONFIG ############
SignalConditioner.implementation=Pass_Through

;Comment: It holds blocks to change data type, filter
        and resample input data.
        Implementation can be selected from
        [Pass_Through] or [Signal_Conditioner].
        [Pass_Through] disables this block and
        the following blocks which are unnecessary
        for L1 C/A.

;########## DATA_TYPE_ADAPTER CONFIG ############
DataTypeAdapter.implementation=Pass_Through

;########## INPUT_FILTER CONFIG ############
InputFilter.implementation=Pass_Through

;########## RESAMPLER CONFIG ############
Resampler.implementation=Pass_Through



;########## CHANNELS GLOBAL CONFIG ############
Channels_1C.count=6
;Comment: count- Number of available
        GPS L1 C/A satellite channels.

Channels.in_acquisition=1
;Comment: in_acquisition- Number of channels
        simultaneously acquiring for the whole receiver,
         wihch is closely related to computation burden.

Channel.signal=1C
;Comment: signal is chosen 1C
```

```
                for L1 C/A signal reception.

;########## SPECIFIC CHANNELS CONFIG ######
Channel0.signal=1C
Channel1.signal=1C
Channel2.signal=1C
Channel3.signal=1C
Channel4.signal=1C
Channel5.signal=1C
;Comment: The options are specific to each channel
        and overwrite the generic options.

Channel0.satellite=1
Channel1.satellite=4
Channel2.satellite=10
Channel3.satellite=25
Channel4.satellite=26
Channel5.satellite=31
;Comment: satellite- Satellite PRN ID for this channel.
        Disable this option for random search

;########## ACQUISITION GLOBAL CONFIG ############
Acquisition_1C.item_type=gr_complex
Acquisition_1C.if=0
;Comment: if is intermediate frequency.
        In this work, we set it at zero.

Acquisition_1C.coherent_integration_time_ms=1
;Comment: coherent integration time is 1 ms
        which can be adjusted based on signal strength.

Acquisition_1C.implementation=GPS_L1_CA_PCPS_Acquisition
Acquisition_1C.threshold=0.01
;Comment: threshold is Acquisition threshold which
        can be adjusted based on signal strength.
```

```
Acquisition_1C.doppler_max=10000
Acquisition_1C.doppler_step=500
Acquisition_1C.max_dwells=1

;########## TRACKING GLOBAL CONFIG ############
Tracking_1C.implementation=GPS_L1_CA_DLL_PLL_Tracking
Tracking_1C.item_type=gr_complex
Tracking_1C.if=0
;Comment: if is intermediate frequency.
        In this work, we set it at zero.

Tracking_1C.dump=true
Tracking_1C.dump_filename=./tracking_ch_
;Comment: file dump is enabled in order to analyze
        tracking result in following sections.

Tracking_1C.pll_bw_hz=30.0;
Tracking_1C.dll_bw_hz=4.0;
Tracking_1C.order=3;
Tracking_1C.early_late_space_chips=0.5;

;########## TELEMETRY DECODER GPS CONFIG ############
TelemetryDecoder_1C.implementation
                =GPS_L1_CA_Telemetry_Decoder
TelemetryDecoder_1C.dump=false
TelemetryDecoder_1C.decimation_factor=1;
;Comment: the signal decoding is done using the
        algorithm developed by Fernandez at el., [10].

;########## OBSERVABLES CONFIG ############
Observables.implementation=Hybrid_Observables
Observables.dump=true
Observables.dump_filename=./observables.dat
;Comment: Observable block is to compute from channels
        the GNSS basic measurements. Enable or disable
        the Observables internal binary data file
```

```
        logging [true] or [false].

;########## PVT CONFIG #############
PVT.implementation=RTKLIB_PVT
PVT.positioning_mode=PPP_Static
PVT.iono_model=OFF
PVT.trop_model=Saastamoinen
PVT.output_rate_ms=100
PVT.display_rate_ms=500
PVT.dump_filename=./PVT
PVT.nmea_dump_filename=./gnss_sdr_pvt.nmea;
PVT.flag_nmea_tty_port=false;
PVT.nmea_dump_devname=/dev/pts/4
PVT.flag_rtcm_server=true
PVT.flag_rtcm_tty_port=false
PVT.rtcm_dump_devname=/dev/pts/1
;Comment: since our focus is on the data from
        observable block, this is not discussed much.
        However, it should be there in order
        to process the real-time reception.
```

3.1.3 L2 Signal

The GPS L2 signal comprises L2C, P(Y) code and the M-Code centered at carrier frequency of 1227.60 MHz (see Figure 3.2). The L2 Civilian (L2C) signal is the second civilian GPS signal, designed specifically to meet commercial needs. The first GPS satellite featuring L2C launched in 2005. Since then, every fielded GPS satellite has included an L2C transmitter and currently L2C is broadcasting from 19 satellites. This is the second highest number of available civilian signals and this is why it is selected for our work to develop an ionospheric sounding system. The L2C comprises L2 Civil Moderate (L2CM) and L2 Civil Long (L2CL). These two signals are time multiplexed so that the resulting chipping rate is twice as high as that of each individual signal. In this work, the L2CM signal is selected for use. It is transmitted by the IIR-M, IIF, and subsequent blocks. The PRN of the

L2CM signal is 20 ms in length at a chipping frequency of 511.5 kHz with 10230 chips. The technical characteristics of the L2CM signal are summarized in the second column of Table 3.1 [21]. Due to the fact that L2CM has 20 times greater chip length than L1 C/A, it requires more stable oscillators than the internal reference oscillator embedded in the USRP N210. We use the Jackson Lab Fury external oscillator to provide the required stable reference.

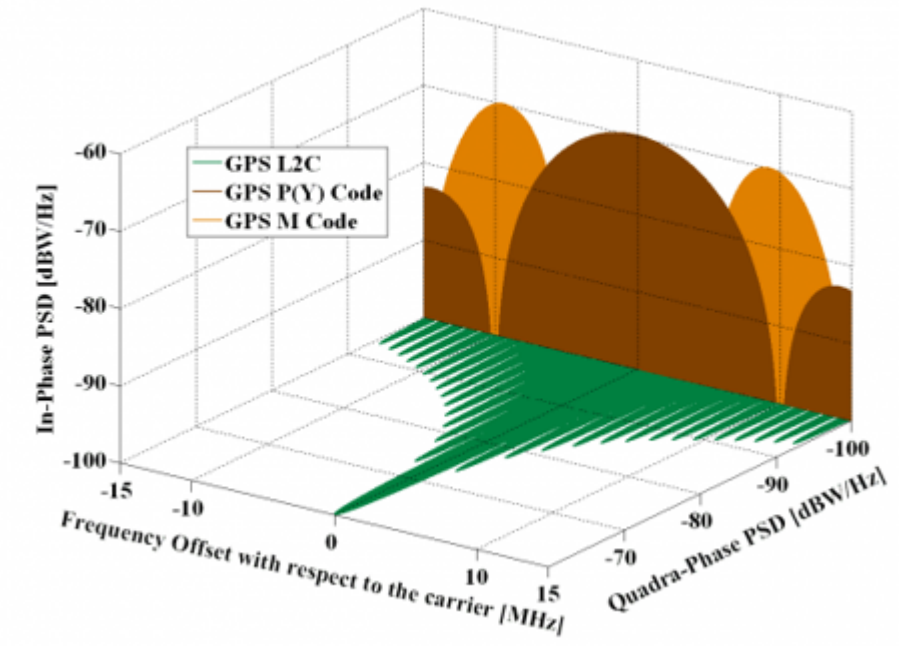

Figure 3.2: L2 Signal Spectrum

3.1.4 L2 Signal Configurations

The following source code specifies the configurations for receiving the L2CM signal, and general information about each block is given in section 2.3. Comments are attached inside of the source code for important details.

```
[GNSS-SDR]

;######### GLOBAL OPTIONS ##################
GNSS-SDR.internal_fs_sps=2000000
```

```
;########## SIGNAL_SOURCE CONFIG ############
SignalSource.implementation=UHD_Signal_Source
SignalSource.device_address=192.168.40.4
;Comment: USRP address needs to be specified.

SignalSource.item_type=gr_complex
SignalSource.sampling_frequency=2000000
;Comment: sampling_frequency is chosen 2 MHz
        because of L2CM bandwidth.

SignalSource.freq=1227600000
;Comment: freq is chosen 1.2276 GHz
        which is L2 center frequency.

SignalSource.gain=60
;Comment: gain is set to 60 dB at the daughterboard.

SignalSource.subdevice=A:0
;Comment: subdevice is RX portion of the USRP.

SignalSource.clock_source=external
;Comment: since we synchronize two USRPs with GPSDO,
        clock_source needs to be external.
        Also, L2CM requires higher stability.

SignalSource.samples=0
SignalSource.repeat=false
SignalSource.dump=false
SignalSource.dump_filename=../data/signal_source.dat
SignalSource.enable_throttle_control=false

;########## SIGNAL_CONDITIONER CONFIG ############
SignalConditioner.implementation=Pass_Through
;Comment: It holds blocks to change data type, filter
        and resample input data. implementation can be
        selected from [Pass_Through] or
```

```
        [Signal_Conditioner]. [Pass_Through] disables
        this block and the following blocks
        which are unnecessary for L2CM.


;########## DATA_TYPE_ADAPTER CONFIG #############
DataTypeAdapter.implementation=Pass_Through

;########## INPUT_FILTER 0 CONFIG #############
InputFilter.implementation=Pass_Through

;########## RESAMPLER CONFIG #############
Resampler.implementation=Pass_Through

;########## CHANNELS GLOBAL CONFIG #############
Channels_2S.count=6
;Comment: count- Number of available
        GPS L1 C/A satellite channels.

Channels.in_acquisition=1

Channel0.signal=2S
Channel1.signal=2S
Channel2.signal=2S
Channel3.signal=2S
Channel4.signal=2S
Channel5.signal=2S

Channel0.satellite=1
Channel1.satellite=4
Channel2.satellite=10
Channel3.satellite=25
Channel4.satellite=26
Channel5.satellite=31
;Comment: satellite- Satellite PRN ID for this channel.
        Disable this option for random search.
```

```
;########## ACQUISITION GLOBAL CONFIG ############
;# GPS L2C M
Acquisition_2S.dump=false
Acquisition_2S.dump_filename=./acq_dump.dat
Acquisition_2S.item_type=gr_complex
Acquisition_2S.if=0
Acquisition_1C.coherent_integration_time_ms=10
;Comment: coherent integration time is 10 ms
        which can be adjusted based on signal strength.
        L2CM is weaker than L1 C/A signal
        so it is chosen to 10 ms.

Acquisition_2S.implementation=GPS_L2_M_PCPS_Acquisition
Acquisition_2S.threshold=0.005
;Comment: threshold is Acquisition threshold which
        can be adjusted based on signal strength

Acquisition_2S.doppler_max=10000
Acquisition_2S.doppler_min=-10000
Acquisition_2S.doppler_step=100
Acquisition_2S.max_dwells=1

;########## TRACKING GLOBAL CONFIG ############
Tracking_2S.implementation=GPS_L2_M_DLL_PLL_Tracking
Tracking_2S.item_type=gr_complex
Tracking_2S.if=0
Tracking_2S.dump=true
Tracking_2S.dump_filename=./tracking_ch_
Tracking_2S.pll_bw_hz=1.5;
Tracking_2S.dll_bw_hz=0.3;
Tracking_2S.order=3;
Tracking_2S.early_late_space_chips=0.5;

;########## TELEMETRY DECODER GPS CONFIG ############
TelemetryDecoder_2S.implementation
```

```
                =GPS_L2C_Telemetry_Decoder
TelemetryDecoder_2S.dump=false
;Comment: the signal decoding is done using the
        algorithm developed by Fernandez at el., [10].

;########## OBSERVABLES CONFIG ############
Observables.implementation=Hybrid_Observables
Observables.dump=false
Observables.dump_filename=./observables.dat
;Comment: Observable block is to compute from channels
        the GNSS basic measurements. Enable or disable
        the Observables internal binary data file
        logging [true] or [false]

;########## PVT CONFIG ############
PVT.implementation=RTKLIB_PVT
PVT.positioning_mode=PPP_Static
PVT.iono_model=OFF
PVT.trop_model=OFF
PVT.output_rate_ms=100
PVT.display_rate_ms=500
PVT.dump_filename=./PVT
PVT.nmea_dump_filename=./gnss_sdr_pvt.nmea;
PVT.flag_nmea_tty_port=false;
PVT.nmea_dump_devname=/dev/pts/4
PVT.flag_rtcm_server=false
PVT.flag_rtcm_tty_port=false
PVT.rtcm_dump_devname=/dev/pts/1
PVT.dump=false
;Comment: since our focus is on the data from
        observable block, this is not discussed much.
        However, it should be there in order
        to process the real-time reception.
```

3.2 Result of the Acquisition and Tracking

The role of an Acquisition block is the detection of signals coming from a given GNSS satellite. In case of a positive detection, it should provide coarse estimation of the code phase and the Doppler shift of the signal, at a level accurate enough to initialize the delay and phase tracking loops. The Tracking block continually receives the data stream from the Acquisition block with code lag and coarse Doppler frequency. Using PLL and DLL techniques, this block consistently tracks the code phase, Doppler shift, and carrier phase. It then provides modulated data to the Decoder block. The acquisition and tracking results with configuration details are discussed in this section.

The signal configurations provided in section 3.1.2 for L1, and in section 3.1.4 for L2, provide details of the navigation algorithm. The acquisition and tracking results of the receiver are verified by examining three parameters: (1) Doppler frequency, (2) in-phase vs. quadrature, (3) C/N_0 amplitude.

As shown in Figure 3.3, the interface of the GNSS-SDR is able to provide the channel information, C/N_0, and receiving time. Depending on the configuration setup, the interface is also able to provide not only acquisition and tracking results but also the WGS-84 format navigation solution results in the terminal directly as shown in Figure 3.4. Figure 3.4 shows the PVT solution from the L1 C/A signal which provides latitude, longitude, and height information, and the solution indicates 40.11°, -88.22°, and 205 m, respectively.

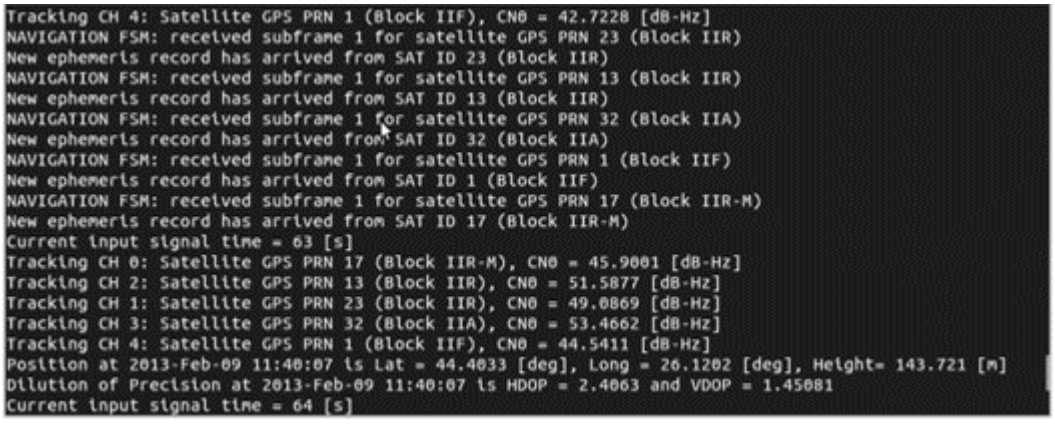

Figure 3.3: Example of Acquisition and Tracking Interface

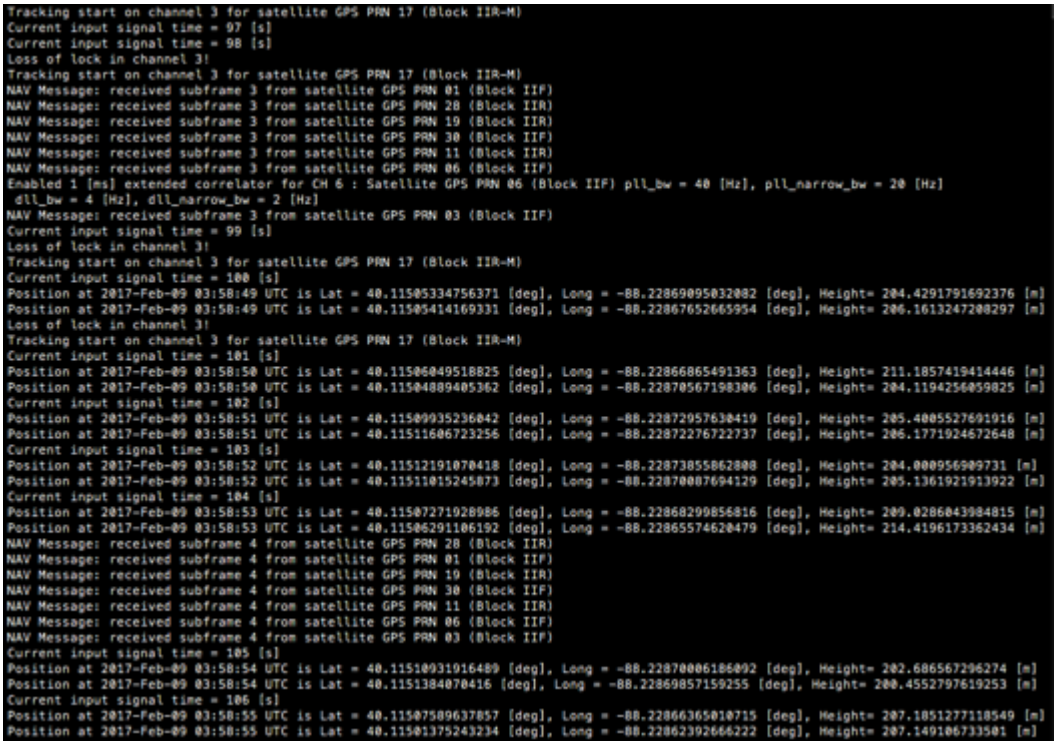

Figure 3.4: Example of Position Velocity and Time Interface

Figures 3.5 through 3.9 plot the acquisition and tracking results of the GPS L1 C/A and GPS L2CM signals. Figure 3.5 shows L1 and L2 Doppler frequency of PRN 1 around -1600 Hz and -1200 Hz respectively. Since we are tracking the same satellite, these two Doppler frequencies must be similar and continuous, and they make sense based on the relationship between observed frequency f and emitted frequency f_i as:

$$f_d = f - \left(\frac{c + v_r}{c + v^{(s)}}\right) f_i \tag{3.1}$$

where:

- f is the observed frequency
- f_i is the emitted frequency
- f_d is the Doppler frequency
- c is speed of light (299,792.458 m/s)
- v_r is the speed of receiver

- $v^{(s)}$ is the speed of satellite

Since the receiver is tracking the same satellite, the $\left(\frac{c+v_r}{c+v^{(s)}}\right)$ term should be the same for L1 and L2. The relationship between two Doppler frequencies can be represented simply:

$$f_{d_{L2}} = \frac{f_{L1} + f_{d_{L1}}}{f_{L1}} f_{L2} - f_{L2} \tag{3.2}$$

In order to verify the Doppler frequency result that is caused from the same satellite, L2 Doppler frequency is calculated based on the Equation 3.2 with the rough estimate of L1 Doppler frequency as -1600.00 Hz, and the result is -1246.75 Hz which is shown in Figure 3.5. The L1 Doppler frequency shows some jitter which is caused by the brief C/N_0 reception degradation for a short amount of time as shown in Figure 3.6. However, since the degradation is recovered before hurting the tracking loop, L1 signal is robust enough to give steady navigation results compared to the L2 signal.

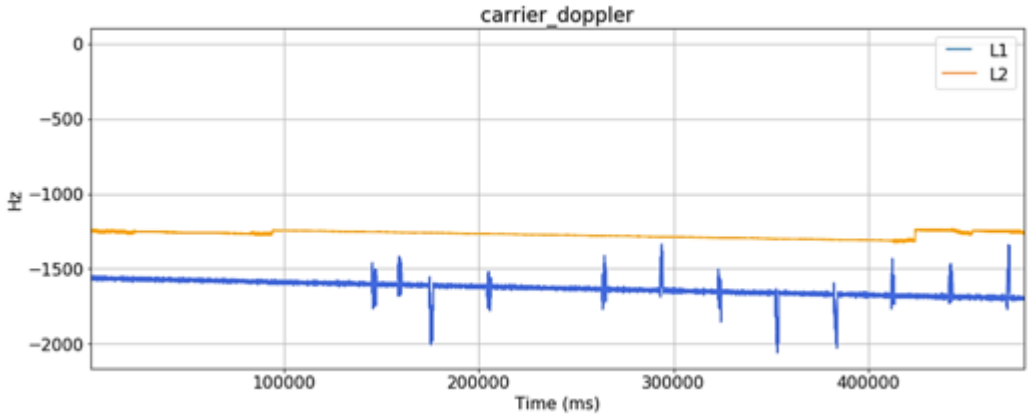

Figure 3.5: L1 and L2 Doppler Frequency of PRN 1

Figure 3.6 shows C/N_0 amplitudes which must be higher than 25 dB-Hz to keep tracking the satellite. This is a threshold that user can adjust in the configuration. Typical C/N_0 for the L1 and L2 signals is around 37 to 45 dB-Hz. As shown in Figure 3.6, C/N_0 amplitudes for the L1 and L2 signal are around 50 dB-Hz and 45 dB-Hz, respectively, as expected. This means that the carrier power for each signal is sufficient to overcome the noise power and the signals are recognizable. However, around 300 sec, the L2 signal

degrades significantly and is not recovered for a relatively long time, which hurts the tracking loop. The influence of L2 signal reception degradation on overall results will be discussed in Chapter 4.

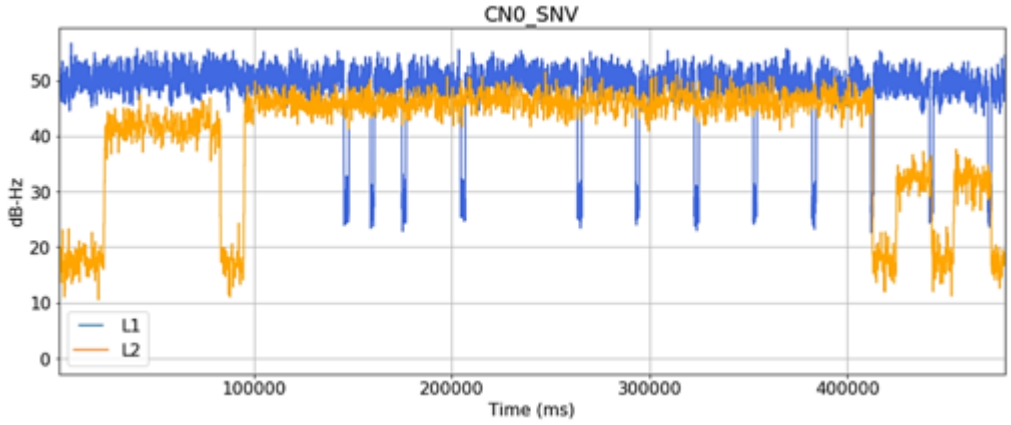

Figure 3.6: C/N_0 Amplitude L1 and L2 of PRN 1

The integration interval used in both the FLL and PLL is 1 ms. FLL is used to lock the incoming signals first, then the PLL is used to refine the frequency and phase. After the signals have been tracked, the software receiver will start to decode the navigation messages. Figure 3.7 shows the in-phase vs. quadrature of L1 and L2 which is the final output of the Tracking block. Since both L1 and L2 employ BPSK(1) modulations as shown in Table 3.1 row 7, there should be two big clouds around +1 and -1.

The Doppler shift frequency changed slowly and linearly after being tracked. The phase transition of demodulated data bits can be clearly viewed in Figure 3.8 and Figure 3.9. Figure 3.9 shows overall data bit transitions that we collected for PRN 1. In Figure 3.8, zoomed in data bit transition is plotted over 1000 ms (50 bit of data), which can be decoded into the navigation message from the Decoder block.

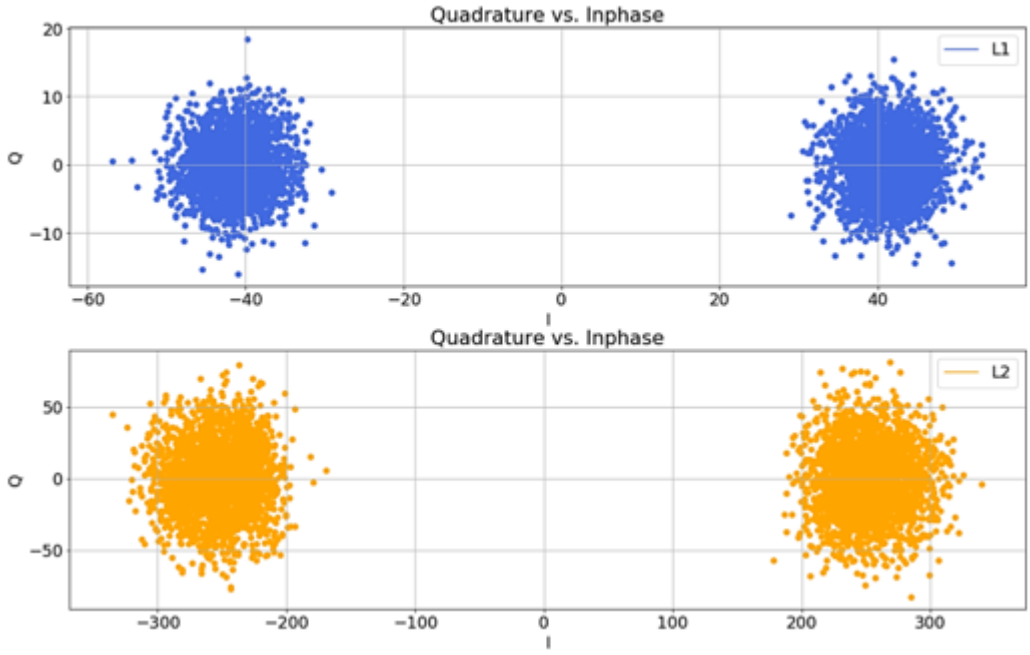

Figure 3.7: In-Phase vs. Quadrature of PRN 1

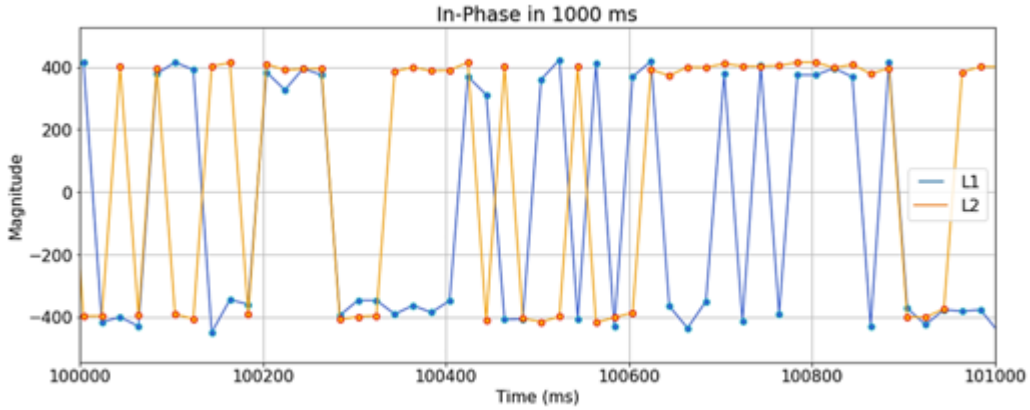

Figure 3.8: In-Phase Over 1 sec L1 and L2 of PRN 1

3.3 Result of the Pseudorange

The main result of the Observable block is the pseudorange measurement, which is generally defined as the difference between the time of reception and the time of transmission of a distinct satellite signal. This corresponds to the

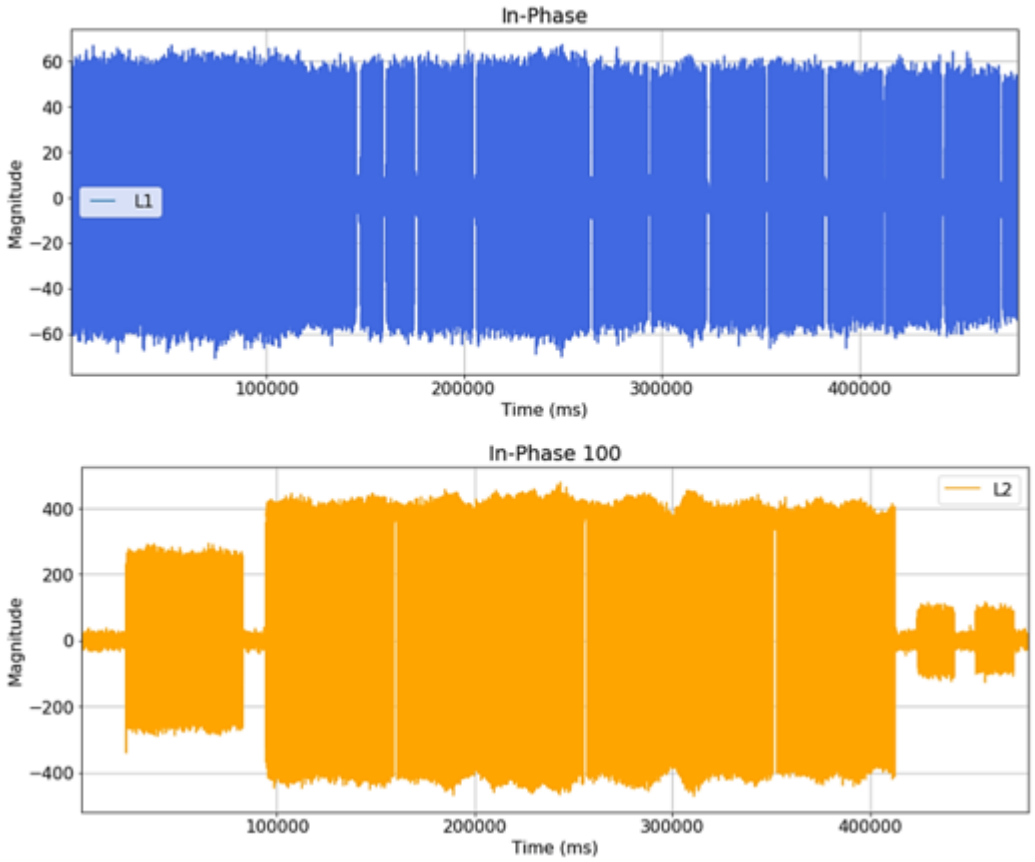

Figure 3.9: In-Phase Over Time L1 and L2 of PRN 1

distance from the receiver antenna to the satellite antenna, including receiver and satellite clock offsets and other biases, such as atmospheric delay and hardware error. Details about ionospheric delay $I_{r,i}$ will be given in Chapter 4. Basic techniques to measure pseudorange are demonstrated in Figure 3.10. For a signal from satellite s in the i-th signal (L1 or L2), the pseudorange $P_{r,i}^{(s)}$ can be expressed by using the signal reception time t_r (in sec) measured by the receiver clock and the signal transmission time t^s (in sec) measured by the satellite clock as shown in Figure 3.10.

The pseudorange equation can be written as:

$$P_{r,i}^{(s)} = c((t_r + dt_r(t_r) - (t^{(s)} + dT^{(s)}(t^{(s)}))) + \epsilon_p \tag{3.3}$$

$$= c(t_r - t^{(s)}) + c(dt_r(t_r) - dT^{(s)}(t^{(s)})) + \epsilon_p \tag{3.4}$$

$$= \rho_r^{(s)} + c(dt_r(t_r) - dT^{(s)}(t^{(s)})) + I_{r,i}^{(s)} + T_r^{(s)} + \epsilon_p \tag{3.5}$$

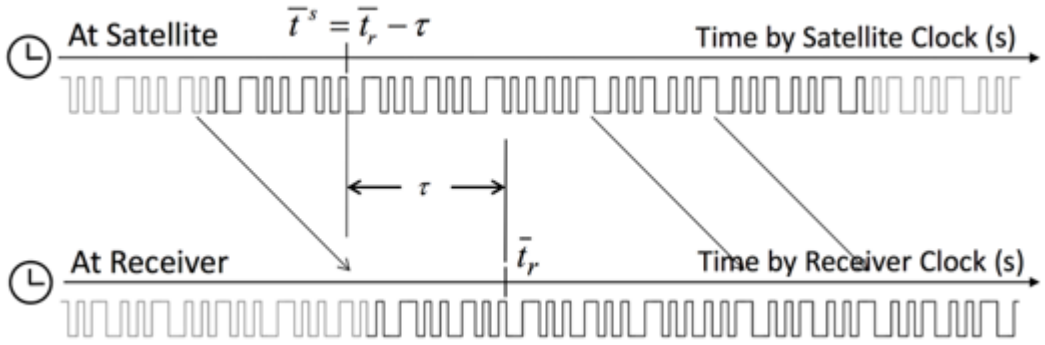

Figure 3.10: Pseudorange Measurement

where:

- $P_{r,i}^{(s)}$ is the pseudorange measurement (in m)
- $P_r^{(s)}$ is the true range from the satellite to the receiver antenna (in m)
- c is the speed of light (in m/s)
- dt_r is the receiver clock offset from GNSS time (in s)
- $dT^{(s)}$ is the satellite clock offset from GNSS time (in s)
- $I_{r,i}^{(s)}$ is the ionospheric delay (in m)
- $Tr^{(s)}$ is the tropospheric delay (in m)
- ϵ_p is the measurement and hardware noise

GNSS-SDR performs pseudorange generation based on setting a common reception time across all channels. The result of this approach is not an absolute pseudorange, but a relative pseudorange with respect to the value (of pseudorange) allocated for a reference satellite. This is possible thanks to the time of week (TOW) information, that is, the epoch conveyed by the navigation message, and the associated reception time t_r, that is, the epoch measured by the receivers time counter, both available for each satellite.

The first step performed by the common reception time algorithm is the selection of a reference satellite: it is the satellite with the most recent TOW (which is the nearest satellite), denoted as TOW_{ref}, whose associated $t_{r_{ref}}$ is taken as the common reception time for all channels. An initial travel time

can be easily calculated in meters considering the speed of light. Then, the pseudoranges for all other satellites are derived by adding the relative-arrival times. Each travel time τ can be computed as:

$$\tau^{(s)} = \Delta TOW^{(s)} + \Delta t_r^{(s)} + \tau_{ref} = TOW^{(s)} - TOW_{ref} + t_r^{(s)} - t_{r_{ref}} + \tau_{ref} \quad (3.6)$$

where:

- $\Delta TOW^{(s)}$ is the difference between the reference TOW_{ref} and the current TOW of the s-th satellite
- $\Delta t_r^{(s)}$is the time elapsed between the reference $t_{r_{ref}}$ and the actual receiver time

Also, in the process of the common reception time algorithm, two-point linear interpolation using adjacent values is implemented for smoothing the calculation of pseudorange [10]. Figure 3.11 shows the pseudorange measurements of the L1 C/A and L2CM signal of PRN 1 with reference satellite 32. We expect a smaller difference around 10 m, with the same rate of change for the two measurements. However, Figure 3.11 shows larger pseudorange difference, about 150 meter, at the maximum which also includes multipath and hardware bias. The pseudorange measurements are relatively smooth as shown in Figure 3.11, and the difference in terms of ionospheric delay will be discussed in the next chapter.

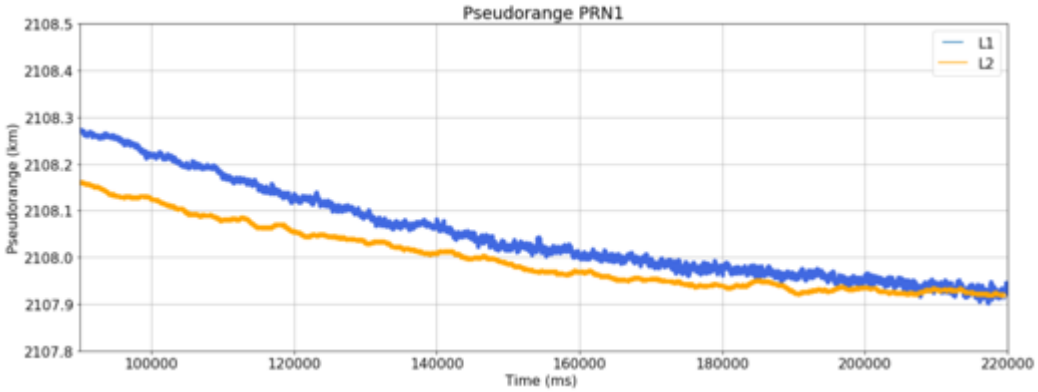

Figure 3.11: Pseudorange Measurement

CHAPTER 4

POSSIBLE IMPLEMENTATION OF IONOSPHERIC SOUNDING SYSTEM

The increase in the measured pseudorange due to the ionosphere delay represents one of the largest sources of error in positioning using a GNSS receiver. This delay can be characterized by a measurement of the total electron content (TEC) between GPS receiver and satellite, which is achieved using dual frequency measurements. When making simultaneous measurements of both GPS L1 C/A and GPS L2C signals, based on the calculation from the dispersion relation, the receiver enables ionospheric correction. Using the dual frequency technique, civilians can measure and remove this delay rather than rely on a model of the expected delay, allowing them to enjoy the same accuracy as the military who have had dual-frequency capabilities. This chapter contains three sections: (1) TEC derivation from dual frequency GNSS measurements, (2) TEC measurement result and (3) measurement result discussion. The TEC derivation is discussed in order to provide a mathematical foundation of the dual-frequency measurement for TEC. The TEC measurement result demonstrates the possible implementation of a USRP-based GNSS receiver to perform TEC measurement.

4.1 TEC Derived from Dual Frequency GNSS Signal

The TEC derived from GNSS is typically calculated from the dispersion relation for a collisionless plasma,

$$k = \frac{\omega}{c}\sqrt{1 - \frac{\omega_p^2}{\omega^2}} \tag{4.1}$$

where:

- k is phase constant/wavenumber of collisionless plasma medium

- $\omega_p = \sqrt{\frac{Ne^2}{m\epsilon_0}}$ is the plasma frequency which is a function of the electron density N
- ω is the carrier frequency
- c is speed of light (299,792.458 m/s)

The wavenumber k is a function of the carrier frequency ω and the electron density N. Since the GNSS satellites are far away from the receiver, it is a valid assumption to treat the incoming signal as a uniform plane wave. The phase velocity and group velocity of a uniform plane wave can be described by:

$$v_\phi = \frac{\omega}{k} = \frac{c}{\sqrt{1 - \frac{\omega_p^2}{\omega^2}}} \tag{4.2}$$

$$v_g = \frac{\delta\omega}{\delta k} = \frac{c}{\sqrt{1 - \frac{\omega_p^2}{\omega^2}}} \tag{4.3}$$

where v_ϕ is phase velocity and v_g is group velocity. The incurred delay during the propagation, from receiver to satellite, due to the dispersive region, is

$$\Delta t = \int_\rho \frac{1}{c}\delta\rho - \int_\rho \frac{1}{v_g}\delta\rho \tag{4.4}$$

$$\approx \int_\rho \frac{1}{c}\delta\rho - \int_\rho \frac{1}{c}(1 + \frac{\omega_p^2}{2\omega^2})\delta\rho \tag{4.5}$$

$$= -\frac{e^2}{2c\omega^2\epsilon_0 m}\int_\rho N\delta\rho \tag{4.6}$$

where:

- $\int_\rho N\delta\rho$ is TEC of the signal propagation
- $\frac{1}{v_g} \approx 1 + \frac{\omega_p^2}{2\omega^2}$ is used because GPS frequencies L1 (1.57542 GHz) and L2 (1.2276 GHz) are significantly higher than plasma frequency with the maximum around 10 MHz
- e is electric charge carried by a single electron $1.60217662 \times 10^{-19}$ coulombs

- m is mass of electron $9.10938356 \times 10^{-31}$ kg
- ϵ_0 is vacuum permittivity $8.854187817 \times 10^{-12}$ F/ m

The direct measurement of Δt is not implemented in general GNSS receivers. However, the difference in the delay at two frequencies, $\Delta t_{L1} - \Delta t_{L2}$ can be measured:

$$\rho_{L1} - \rho_{L2} = c(\Delta t_{L1} - \Delta t_{L2}) \tag{4.7}$$

$$= -\frac{e^2}{2c\epsilon_0 m} \frac{\omega_{L1}^2 - \omega_{L2}^2}{\omega_{L1}^2 \omega_{L2}^2} \int_\rho N\delta\rho \tag{4.8}$$

from which the TEC can be calculated as:

$$\int_\rho N\delta\rho = TEC_\rho = \frac{2c\epsilon_0 m}{e^2} \frac{\omega_{L1}^2 \omega_{L2}^2}{\omega_{L1}^2 - \omega_{L2}^2} (\rho_{L1} - \rho_{L2}) \tag{4.9}$$

TEC is the column density of electrons measured in electrons per m^2 (1 TECU=10^{16} electrons per m^2). 1 TECU of electrons induces a delay of 0.542 ns resulting in a 0.163 m error in the pseudorange measurement on the L1 signal. On L2, the delay is 0.890 ns which turns out to be 0.267 m error. TEC ranges about 0-10 TECU (0 1.6 m error) at night, and 20 - 60 TECU during the day (3-10 m error). It can thus readily be seen that roughly every excess 10 cm of pseudorange difference on L2- L1 corresponds to 1 TECU of electron content, or more simply,

$$TEC_\rho = \frac{\rho_{L1} - \rho_{L2}}{0.105 \times 10^{-16}} \tag{4.10}$$

where the pseudorange measurements, ρ_{L1} and ρ_{L2}, are provided in meters.

Similarly, the GPS carrier phase can be used to derive TEC based on v_ϕ instead of v_g, because the phase of the radio wave advances during propagation through a plasma by an equivalent distance as the group velocity is retarded. After converting phase from radians to meters for the L1 and L2 wavelengths, the phase TEC counterpart to Equation 4.9 is written as

$$TEC_\phi = \frac{-\phi_{L1} + \phi_{L2}}{0.105 \times 10^{-16}} \tag{4.11}$$

Because carrier phase is measured with far greater precision than pseudor-

anges derived from code correlation, GPS carrier phase derived TEC provides a smooth and precise, albeit relative, measurement of ionospheric TEC. The relativity is due to ambiguities in the total number of wave cycles between satellite and receiver. Excluding effects such as multipath and hardware biases, the code derived TEC in Equation 4.9 provides an absolute yet noisy measurement of TEC, where this noise is due to the inherent meter-level precision in pseudorange measurements.

4.2 TEC Measurement Result

In this section, the measurement result demonstrates the possible implementation of USRP-based GNSS receiver for TEC measurement. Pseudorange and carrier phase measurements from the L1 and L2 signals are calculated to derive TEC as described above. The measurement was performed on December 7th 2017 UTC 22:16 and shows a short amount of time, about 2 min. Observable block discontinues the pseudorange data collection if the tracking is lost due to the lack of signal robustness. So for the investigation purpose, we revisit the result of tracking result from previous session, which will be shown in the section 4.3. A longer data collection time was not possible due to instability of the captured L2 signal in the USRP.

4.2.1 Differencing Pseudorange Measurement

Figure 4.1 shows TEC calculated from the pseudorange measurement. As in Figure 3.10, the difference between pseudoranges of L1 and L2 is greater than expected, but the overall trends over a short period of time are reasonable. Since we use the common reception time algorithm in section 3.3, we are not able to compare the point to point pseudorange differences to calculate TEC, rather we need to compare the difference of the difference between observed and reference pseudorange for Δ TEC. From observed PRN and reference PRN for the L1 and L2 at each time step, Δ TEC can be calculated. For example, two delta pseudorange can be defined as follows: $\Delta\rho_{L1}$ is $(\rho_{L1_{observed}} - \rho_{L1_{reference}})$ and $\Delta\rho_{L2}$ is $(\rho_{L2_{observed}} - \rho_{L2_{reference}})$. Then we need to compare the $\Delta\rho_{L1}$ and $\Delta\rho_{L2}$ in order to calculate ΔTEC. If the stability of the system allows, a longer period of pseudorange collection will provide

us a chance to compare overall trends with models of the ionosphere or TEC measurement derived from other reference receivers.

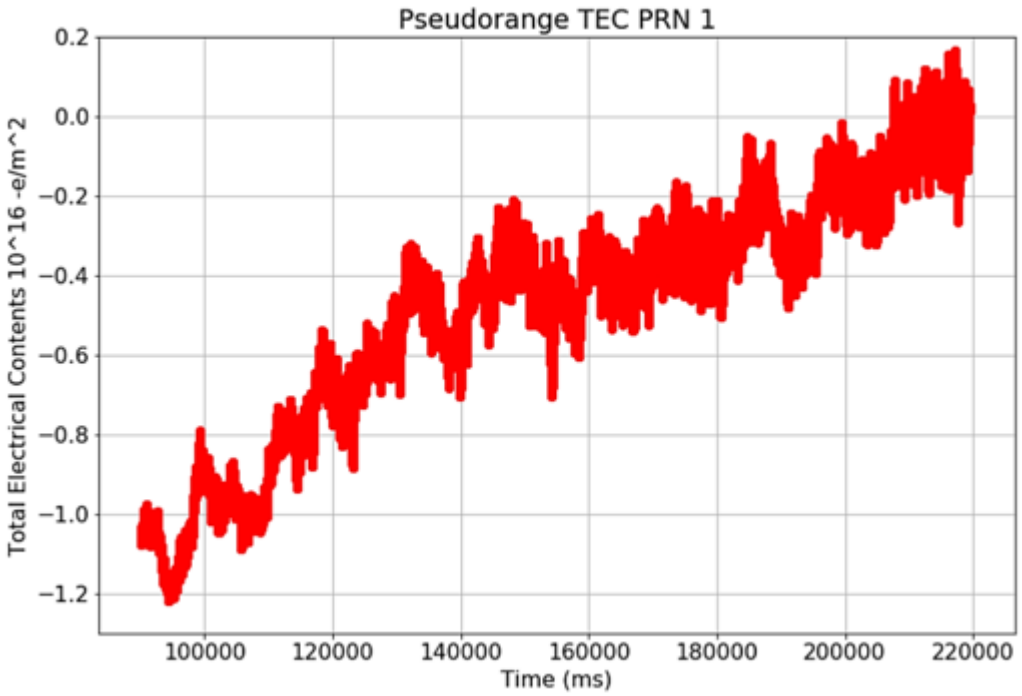

Figure 4.1: TEC Measurement from Pseudorange Differencing

4.2.2 Differencing Carrier Phase measurement

Figure 4.2 shows the TEC measurement derived from carrier phase measurement. As we anticipated from the previous section, carrier phase provides much smoother shape of TEC and expected results. The Trend is closely matched with pseudorange result in Figure 4.1.

4.2.3 Measurement Result Discussion

The results in Figures 4.1 and 4.2 indicate that the current state of the USRP based GNSS system is not accurate and robust enough to make an exact TEC measurement: we believe this is due to a stability issue on the measurement of the L2 signal.

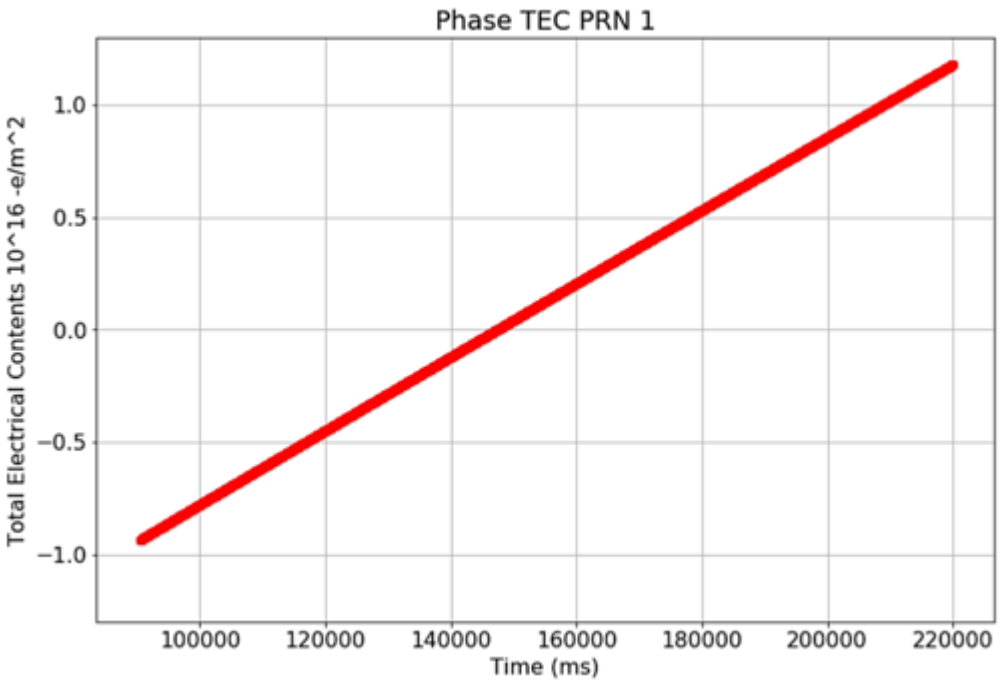

Figure 4.2: TEC Measurement from Phase Differencing

We start to analyze the issue of the L2 signal by looking at the L1 signal result. Observable block generates the pseudorange data only when tracking is robust and decoder block is able to decode the data bits which is why we only have a short period of TEC measurements as shown in Figure 4.1 and Figure 4.2. We revisit the tracking results in section 3.2 for PRN 1 in order to investigate the issue. We concentrate on a different time period than shown in previous Figures because of the longer duration of the tracking result.

As shown in Figure 4.3, C/N_0 shows a huge dip below 20 dB-Hz around 410 sec while the tracking threshold of C/N_0 is 25 dB-Hz. C/N_0 is the first factor that influences the rest of the tracking results. C/N_0 is an indicator of signal reception comparing the carrier power level with noise level as shown in Equation 2.3. This hurts the carrier lock test for the tracking shown in Figure 4.4. In the tracking loop, the carrier lock is tested by two indicators: (1) code lock and (2) carrier lock. As shown in Figure 4.4, the carrier lock test varies from 1 to -1 where 1 means the tracking loop has perfect lock on the carrier and vice versa, where the threshold is at 0.75 for tracking. About 10 s after the degradation of C/N_0, the carrier lock test indicates that the receiver loses the tracking of the signal where test indicators are below

0.75 for about 60 sec. Figure 4.5 shows relatively small jitters of the Doppler frequency for PRN 1 at around 425 sec as an after-effect of signal degradation as well.

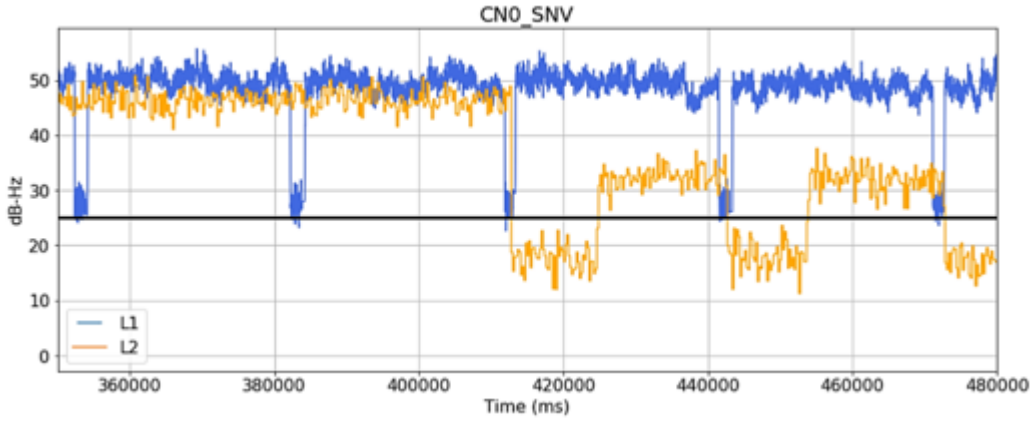

Figure 4.3: C/N_0 Amplitude L1 and L2 of PRN 1

We also investigate the tracking results of the reference PRN. Figures 4.6, 4.7 and 4.8 show the C/N_0 measurement, carrier lock test, and Doppler frequency result of L1C/A and L2CM on PRN 32, respectively. The C/N_0 for this satellite shows a decrease at the same time period as PRN 1 which can be interpreted as meaning that the L2 frequency reception at the antenna is degraded since it affects both signal in a similar way, and, as an after-effect, the carrier lock test failed with poor Doppler frequency estimation as well. At this point, we conclude there is a high possibility that the robustness of the received L2C signal has a serious problem because we encounter this degradation in every single tracking result.

The lack of robustness of the received L2C signal influences the rest of the tracking and measurement results, especially pseudorange and TEC. The observable block discontinues the data collection under the lack of robustness condition. The problem makes it hard to track the same two satellites for a sufficient amount of time: one for the observation, and one for the reference of common reception time algorithm. If the L2C signal reception were more robust, the overall trend of TEC measurement would be able to be compared with measurements or models from the other sources of TEC information. Even though the instability issue with L2 is not resolved in this work, the operating principles and possible implementation are demonstrated. Further

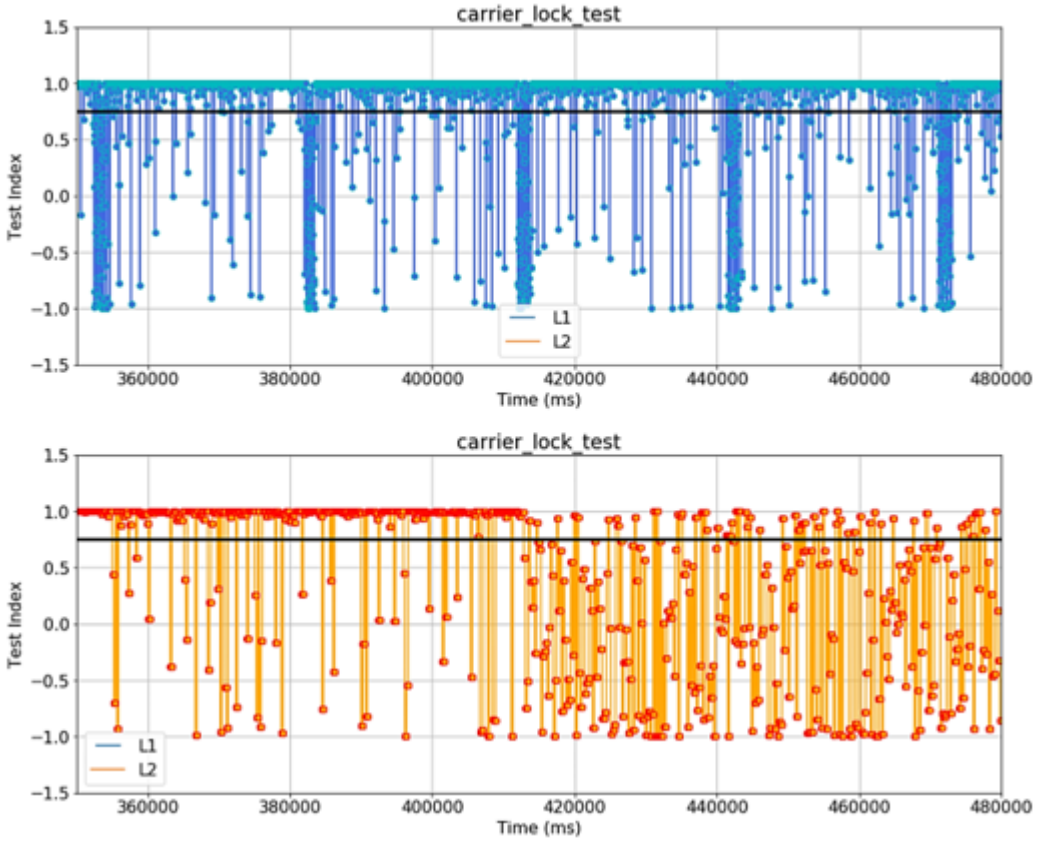

Figure 4.4: Carrier Lock Test for L1 and L2 of PRN 1

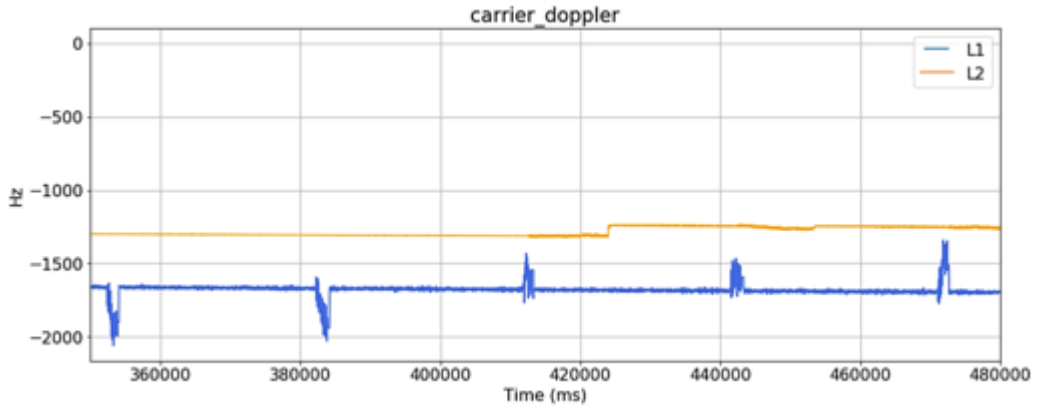

Figure 4.5: L1 and L2 Doppler Frequency of PRN 1

work is needed to address this issue before a USRP-based GNSS receiver can be fully implemented on a USRP-based ionospheric sounder.

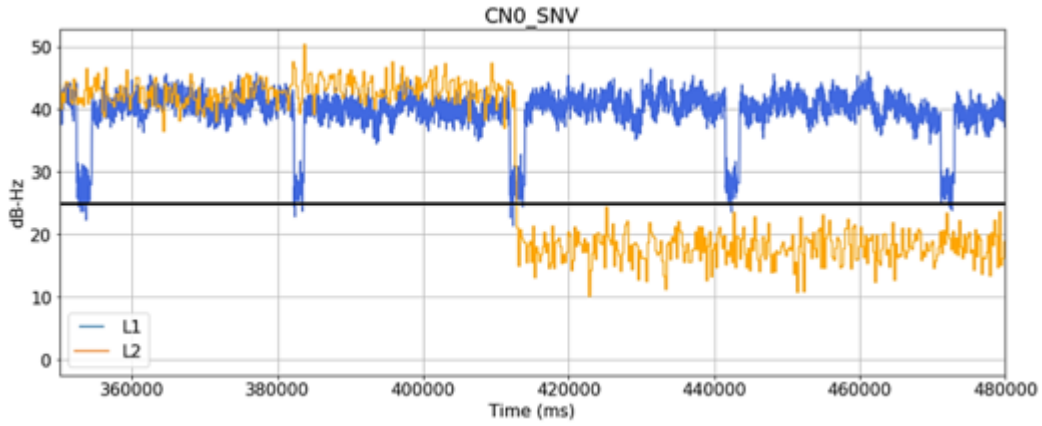

Figure 4.6: C/N_0 Amplitude L1 and L2 of PRN 32

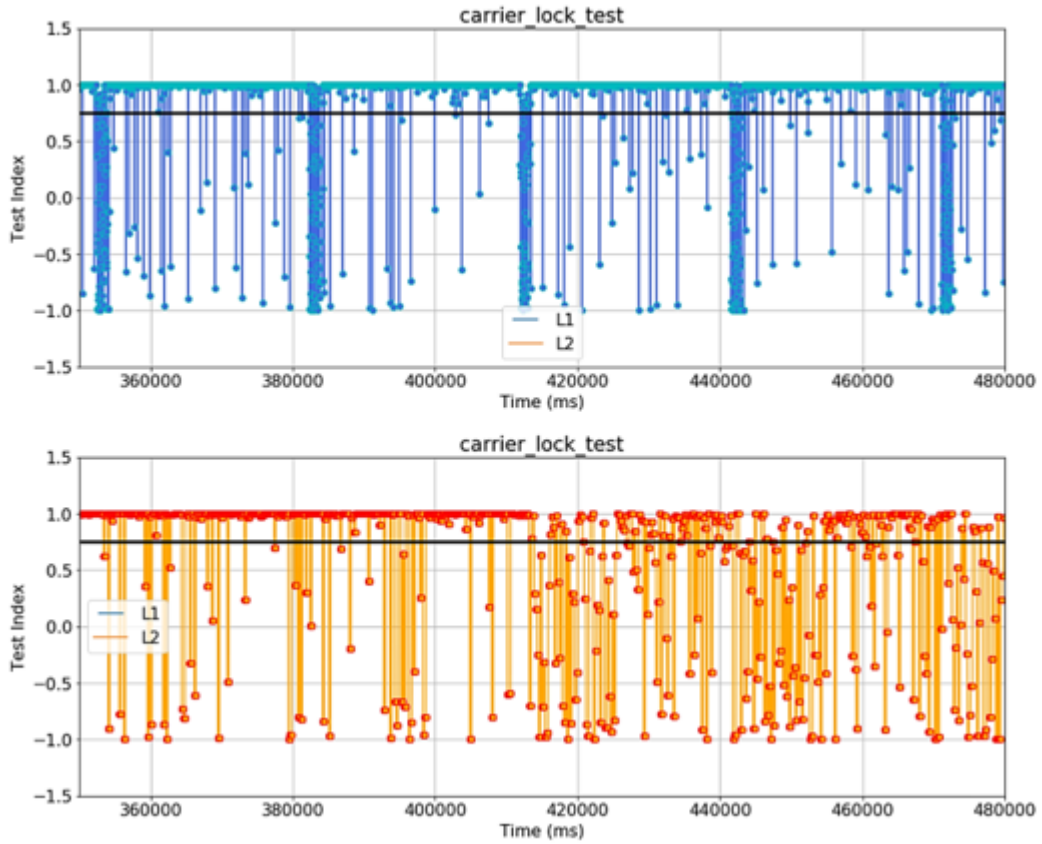

Figure 4.7: Carrier Lock Test for L1 and L2 of PRN 32

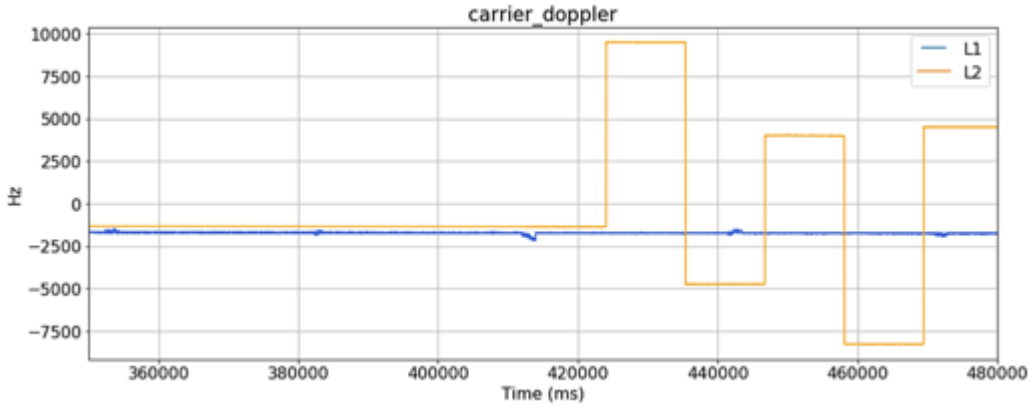

Figure 4.8: L1 and L2 Doppler Frequency of PRN 32

CHAPTER 5

CONCLUSION AND FUTURE WORK

In this work, we have developed two USRP-based real-time GNSS receivers. The receivers have the capability to process both GPS L1 C/A and L2CM signals and provide pseudorange solution - all in real time. The approach, which builds on the USRP N210, makes the receiver flexible, with a reasonable cost. The ability to track both L1 and L2 signals broadcast by GPS opens up the possibility of ionosphere measurements using this system. Ionosphere measurement based on TEC is performed using the pseudorange.

Chapter 2 provides the details of each RF-front-end component, the specification of the USRP N210, and each block in the GNSS-SDR software. The signal plans and results of the navigation solution for the L1 and L2 signals were covered in Chapter 3. Thanks to the advantage of being implemented on the SDR, the data from the acquisition, tracking, and observable blocks of the GNSS SDR were read and visualized to determine the performance of each block from the in-phase vs. quadrature, the doppler frequency, the C/N_0, and the pseudorange measurement. We verified that the SDR implementation works well and can be utilized for ionospheric sounding purposes by generating two different pseudoranges and phase velocities using both the L1 and L2 signals.

In Chapter 4, to measure the ionospheric TEC, mathematical and theoretical approaches are explained. The TEC measurement based on GPS measurements is derived from the dispersion relationship of the collisionless plasma using the differencing of pseudorange and phase velocity GPS measurements. Unfortunately, the TEC measurement using our system did not work as expected because of the instability of the received L2 signal and the fact that only a few seconds of data were available for analysis.

Future work will include a more stable system for the L2 signal and the ability to produce real-time TEC measurement. Once working, the system can be utilized for educational and research purposes. Researchers and stu-

dents can see the effect of changing different configuration parameters on the receiver performance. This will help a lot in understanding the GNSS systems, the ionospheric sounding system, and the signal processing algorithms that work in GNSS and ionosphere-related studies.

REFERENCES

[1] J. Mitola, "Software radios: Survey, critical evaluation and future directions," *IEEE Aerospace and Electronic Systems Magazine*, vol. 8, no. 4, pp. 25–36, 1993.

[2] C. Felita and M. Suryanegara, "5G key technologies: Identifying innovation opportunity," in *QiR (Quality in Research), 2013 International Conference on*. IEEE, 2013, pp. 235–238.

[3] X. Xiong, T. Wu, H. Long, and K. Zheng, "Implementation and performance evaluation of LECIM for 5G M2M applications with SDR," in *Globecom Workshops (GC Wkshps), 2014*. IEEE, 2014, pp. 612–617.

[4] F. Kaltenberger, R. Knopp, N. Nikaein, D. Nussbaum, L. Gauthier, and C. Bonnet, "Openairinterface: Open-source software radio solution for 5G," in *European Conference on Networks and Communications (EUCNC), Paris, France*, 2015.

[5] S. Mathur, S. S. Sagari, S. O. Amin, R. Ravindran, D. Saha, I. Seskar, D. Raychaudhuri, and G. Wang, "Demo abstract: CDMA-based IoT services with shared band operation of LTE in 5G," *arXiv preprint arXiv:1705.06968*, 2017.

[6] D. M. Akos, "A software radio approach to global navigation satellite system receiver design," Ph.D. dissertation, Ohio University, 1997.

[7] K. Borre, D. M. Akos, N. Bertelsen, P. Rinder, and S. H. Jensen, *A Software-Defined GPS and Galileo Receiver: A Single-Frequency Approach*. Springer Science & Business Media, 2007.

[8] S. Peng and Y. Morton, "A USRP2-based reconfigurable multi-constellation multi-frequency GNSS software receiver front end," *GPS Solutions*, vol. 17, no. 1, pp. 89–102, 2013.

[9] L. L. Presti, P. di Torino, E. Falletti, M. Nicola, and M. T. Gamba, "Software defined radio technology for GNSS receivers," in *Metrology for Aerospace (MetroAeroSpace), 2014 IEEE*. IEEE, 2014, pp. 314–319.

[10] C. Fernandez-Prades, J. Arribas, P. Closas, C. Aviles, and L. Esteve, "GNSS-SDR: An open source tool for researchers and developers," in *Proceedings of the 24th International Technical Meeting of The Satellite Division of the Institute of Navigation (ION GNSS 2011)*, 2001, pp. 780–0.

[11] L. Dyrud, A. Jovancevic, A. Brown, D. Wilson, and S. Ganguly, "Ionospheric measurement with GPS: Receiver techniques and methods," *Radio Science*, vol. 43, no. 6, 2008.

[12] S. Shanmugam, J. Jones, A. MacAulay, and A. Van Dierendonck, "Evolution to modernized GNSS ionospheric scintillation and TEC monitoring," in *Position Location and Navigation Symposium (PLANS), 2012 IEEE/ION*. IEEE, 2012, pp. 265–273.

[13] V. Romano, G. Macelloni, L. Spogli, M. Brogioni, G. Marinaro, and Mitchell, "Measuring GNSS ionospheric total electron content at concordia, and application to L-band radiometers," *Annals of Geophysics*, 2013.

[14] S. Ganguly, A. Jovancevic, A. Brown, M. Kirchner, S. Zigic, T. Beach, and K. M. Groves, "Ionospheric scintillation monitoring and mitigation using a software GPS receiver," *Radio Science*, vol. 39, no. 1, 2004.

[15] N. Linty, R. Romero, F. Dovis, and L. Alfonsi, "Benefits of GNSS software receivers for ionospheric monitoring at high latitudes," in *Radio Science Conference (URSI AT-RASC), 2015 1st URSI Atlantic*. IEEE, 2015, pp. 1–6.

[16] A. Jovancevic, A. Brown, S. Ganguly, M. Kirchner, S. Zigic, L. Scott, and P. Ward, "Reconfigurable dual frequency software GPS receiver and applications," in *ION GPS 2001*, 2001.

[17] NovAtel, "GPS-703-GGG-HV and GPS-703-GGG-HV-N User Guide," 2014, Rev. 2. [Online]. Available: https://www.novatel.com/assets/Documents/Manuals/GPS703GGGHVUserManual.pdf

[18] GPSsource, "S14 Splitter Technical Product Data," 2014, original document from GPSsource. [Online]. Available: https://cdn.shopify.com/s/files/1/0986/4308/ files/1559-TS-GPS-1X4-Splitter-04.pdf

[19] MiniCircuit, "Coaxial Amplifier ZKL-1R5+ and ZKL-1R5," 2015, Rev. A. [Online]. Available: https://www.minicircuits.com/pdfs/ZKL-1R5.pdf

[20] JacksonLabs, "Fury User Guide," 2016, Rev. 1.3. [Online]. Available: http://www.jackson-labs.com/assets/downloads/Fury_user_manual.pdf

[21] J. Sanz Subirana, J. M. Juan Zornoza, and M. Hernandez-Pajares, "GNSS signal," 2011, original document from navipedia.net. [Online]. Available: http://www.navipedia.net/index.php/GNSS_signal